

UNCLASSIFIED

CONFIDENTIAL

RM A54B08

NACA RM A54B08

  
NACA

# RESEARCH MEMORANDUM

THE EFFECT OF LIP SHAPE ON A NOSE-INLET INSTALLATION  
AT MACH NUMBERS FROM 0 TO 1.5 AND A METHOD FOR  
OPTIMIZING ENGINE-INLET COMBINATIONS

By Emmet A. Mossman and Warren E. Anderson

Ames Aeronautical Laboratory

Moffett Field, Calif.

CLASSIFICATION CHANGED

UNCLASSIFIED

To \_\_\_\_\_

**LIBRARY COPY**

By authority of *NASA TPA 9* *Effective*  
Date *9-1-59*  
*NB 11-23-59*

MAY 10 1954

AMES AERONAUTICAL LABORATORY

CLASSIFIED DOCUMENT

This material contains information affecting the National Defense of the United States within the meaning of the espionage laws, Title 18, U.S.C., Secs. 793 and 794, the transmission or revelation of which in any manner to an unauthorized person is prohibited by law.

## NATIONAL ADVISORY COMMITTEE FOR AERONAUTICS

WASHINGTON

May 7, 1954

CONFIDENTIAL

UNCLASSIFIED

UNCLASSIFIED

NACA RM A54B08



3 1176 01434 7851

NATIONAL ADVISORY COMMITTEE FOR AERONAUTICS

RESEARCH MEMORANDUM

## THE EFFECT OF LIP SHAPE ON A NOSE-INLET INSTALLATION

AT MACH NUMBERS FROM 0 TO 1.5 AND A METHOD FOR  
OPTIMIZING ENGINE-INLET COMBINATIONS

By Emmet A. Mossman and Warren E. Anderson

## SUMMARY

An experimental investigation was made at subsonic, transonic, and supersonic speeds of the effect of lip shape on the drag, pressure recovery, and mass flow of a nose-inlet air-induction system. Four lips of varying degrees of bluntness were tested on a fuselage model at Mach numbers of 0 to 1.5 and at angles of attack of  $0^\circ$  to  $12^\circ$ . In general, blunting the lip increased the pressure recovery at all the speeds of this test. The improvement in pressure recovery due to rounding the lip was small at supersonic and at high subsonic speeds, but resulted in marked improvement at the take-off condition. At supersonic speeds in the mass-flow-ratio range of normal operation (0.8 to maximum), going from a sharp lip to a slightly rounded lip had no significant effect on the drag. However, a more blunt lip, typical of a subsonic design, resulted in a considerable increase in drag. The rate of change of drag coefficient with mass-flow ratio was best predicted, in the supersonic speed range, by the theory of Fraenkel.

An analysis was made by combining the pressure recovery and drag force into a single parameter (an effective drag coefficient), and by matching the inlet air flow with an assumed engine air flow. This analytical study showed little difference in the effective drag coefficient for the sharp and slightly rounded lip shapes at supersonic speeds. It was indicated that these inlets can operate efficiently over a wide range of mass-flow ratios at the supersonic speeds investigated, thus simplifying the engine-inlet matching on this particular installation. From the standpoint of higher pressure recovery at take-off and at subsonic speeds, and for better performance (lower effective drag) at supersonic speeds, a slightly rounded lip would be preferable to a sharp lip or a blunt lip for this inlet installation.

~~CONFIDENTIAL~~

UNCLASSIFIED

## INTRODUCTION

As a result of the efforts of a number of investigators, considerable information is available for designing nose-inlet air-induction systems to operate efficiently either in the subsonic or in the supersonic speed regimes (refs. 1, 2, 3, and 4). In general, this information has shown that efficient subsonic operation requires an inlet with a rounded lip, while efficient supersonic operation requires a sharp lip. Although some research has been performed in the transonic and low supersonic speed ranges, where both subsonic and supersonic flow can be present (refs. 5, 6, and 7), not enough information is available for the inlet designer to make an informed compromise between the subsonic and supersonic types of lips. Reference 5 presents data for one rounded and one sharp lip but is considered insufficient for a definite conclusion. In references 6 and 7, sharpening the lips and reducing the external body thickness aft of the lips also reduced the drag, but the effect of lip shape alone was not investigated.

It is the purpose of this report to evaluate the effect of lip shape on the performance of a normal-shock, nose-inlet, air-induction system designed to operate in the subsonic, transonic, and low supersonic speed ranges. The evaluation is made in two parts: (1) an experimental investigation of the drag, pressure-recovery, and mass-flow characteristics of the air-induction system with inlet lips of varying degrees of bluntness, and (2) analysis of the relative merits of the various lip shapes based on a method of engine-inlet matching and optimization which gives an effective drag coefficient. In addition, methods are studied for estimating the variation of net drag with inlet mass-flow ratio.

The experimental tests were made in the Ames 6- by 6-foot supersonic wind tunnel. A description of this wind tunnel is given in reference 8.

## SYMBOLS

a	speed of sound, ft/sec
A	area, sq ft
$A_0$	free-stream tube area, $\frac{W_a}{\rho_0 V_0 g}$ , sq ft
$A_{max}$	maximum fuselage frontal area, 0.2394 sq ft

$$C_D' \quad \text{effective drag coefficient, } \left[ C_D \left( \frac{A_{\max}}{S} \right) \right] +$$

$$\left[ \frac{1}{q_o S} \left( \frac{\frac{\Delta F}{F_{N_{isen}}}}{\frac{\Delta p_t}{p_{t_o}}} \right) \left( 1 - \frac{p_{t_c}}{p_{t_o}} \right) F_{N_{isen}} \right]$$

$C_{D_{pe}}$  pre-entry (or additive) drag coefficient

$C_D$  net drag coefficient,  $\frac{D}{q_o A_{\max}} = C_{D_{pe}} + C_{D_f} + C_{D_p}$

$C_{D_f}$  friction drag coefficient,  $\frac{\text{friction drag}}{q_o A_{\max}}$

$C_{D_p}$  pressure drag coefficient,  $\frac{\text{pressure drag}}{q_o A_{\max}}$

$D$  drag, lb

$\Delta F$   $F_{N_{isen}} - F_N$ , lb

$F_{N_{isen}}$  net thrust with isentropic pressure recovery, lb

$F_N$  net thrust with measured pressure recovery, lb

$g$  acceleration due to gravity, ft/sec<sup>2</sup>

$m$  mass flow, slugs/sec

$m_1/m_o$  mass-flow ratio,  $\frac{\rho_1 A_1 V_1}{\rho_o A_1 V_o}$

$m_{1e}/m_o$  mass-flow ratio,  $\frac{\rho_1 A_1 V_1}{\rho_o A_{1e} V_o}$

$M$  Mach number

$M_1$  entrance Mach number (assuming isentropic flow to station 1),  
 $\frac{W_a}{\rho_1 g A_1 a_1}$

~~CONFIDENTIAL~~

q	dynamic pressure, lb/sq ft
p	pressure, lb/sq ft
$\Delta p_t$	$p_{t_o} - p_{t_c}$ , lb/sq ft
S	assumed wing area, 3.76 sq ft
T	temperature, °R
V	velocity, ft/sec
$W_a$	weight of air, lb/sec
$\alpha$	angle of attack, deg
$\rho$	mass density of air, slugs/cu ft
$\eta$	subsonic diffuser efficiency, $\frac{p_{t_c} - p_1}{p_{t_1} - p_1}$
$\theta$	$\frac{T_t}{T_{std}}$
$\delta$	$\frac{p_t}{p_{std}}$

## Subscripts

o	free stream
1	inlet station (station at minimum duct area)
c	station of compressor entrance
isen	isentropic
le	station at lip leading edge
t	total
s	stagnation station on lip
std	standard sea-level conditions

## APPARATUS AND PROCEDURE

The air-induction model used in the tests (fig. 1) was sting mounted and had no wings or control surfaces. The front portion corresponded to the forward half of a fuselage with a nose inlet, and this section was followed by a cylindrical afterbody. The cylindrical afterbody was selected so that shock waves reflected from the tunnel walls and intersecting this part of the model would not result in pressure changes on the body having force components in the axial direction. Four lip shapes of varying degrees of bluntness were tested, and photographs of the sharp and most blunt lips are shown together with the basic body in figure 2. The lip coordinates are given in figure 3, and the diffuser area variations for each lip are shown in figure 4. The equivalent total cone angle of the diffuser is low, usually less than  $1^\circ$ . The passage at the simulated compressor inlet station corresponded to the entrance of a 1/10-scale J-57 jet engine. For this engine the Mach number at the compressor inlet varies from 0.35 for normal power to about 0.45 for military power plus afterburning.

The model air-induction system was connected to pumps located outside the wind tunnel. A photograph of the model and piping in the wind tunnel is shown in figure 5. The quantity of air flow through the model was regulated by a valve and measured by a standard A.S.M.E. orifice meter. Leakage of air between the model afterbody and the tunnel sting support was minimized by a labyrinth seal; the leakage air flow through the seal was calibrated and amounted to from 0.5 to 2.0 percent of the total air flow. Pertinent corrections were made.

The pressures at the simulated compressor inlet were measured by a rake of 20 total pressure tubes and 2 static pressure tubes, and the pressures at the model exit were measured simultaneously by a rake of 20 total pressure tubes and 4 static pressure tubes (see fig. 1). Model base pressures were measured at 12 points. A three-component strain-gage balance inside the model was used to measure the forces.

Tests were made for a range of mass-flow ratios from 0 to a maximum, angles of attack up to  $12^\circ$ , and Mach numbers of 0, 0.7, 0.8, 0.9, 1.23, 1.35, and 1.50. Except for the static tests ( $M_0 = 0$ ), all experiments were made with a constant tunnel stagnation pressure of 12 pounds per square inch absolute. The corresponding Reynolds number per foot varied from  $3.13 \times 10^6$  to  $3.82 \times 10^6$ .

In the reduction of the data, the forces developed by the internal flow and the base forces were subtracted from the balance measured values. The internal-flow force is defined as the change in total momentum of the entering stream tube from the free stream to the exit of the model, and is thus consistent with the usual definition of jet-engine thrust.

## RESULTS

A comparison of the pressure-recovery characteristics for the four lip shapes is given in figures 6, 7, and 8. The pressure recovery at  $0^\circ$  angle of attack for simulated take-off ( $M_0 = 0$ ), high-subsonic-speed ( $M_0 = 0.7, 0.8, 0.9$ ), and supersonic-speed ( $M_0 = 1.23, 1.35, 1.50$ ) operation is presented in figures 6 and 7. The variation of pressure recovery for three of the lip shapes (lips 2, 3, and 4) with angle of attack is shown in figure 8 for Mach numbers of 0.7 and 0.9. For the angle-of-attack range investigated at supersonic speeds ( $0^\circ$  to  $5^\circ$ ) there was no significant change in the pressure recovery; consequently, only the data at  $0^\circ$  are presented.

The results of the drag measurements are shown in figures 9 and 10. It will be noted that drag coefficients for supersonic speeds only are shown since the drag measurements at subsonic speeds were inconsistent and were considered unreliable. The variation of the drag coefficient with  $m_1/m_0$  for the inlet installation at the angle of attack for minimum drag of these tests is presented in figure 9 for Mach numbers of 1.23, 1.35, and 1.50. Curves similar to those in figure 10, which give the drag coefficient as a function of angle of attack for lips 2 and 3, were used in selecting these angles of attack ( $\alpha = 0^\circ$  for the sharp lips, lips 1 and 2, and  $\alpha = 2.5^\circ$  for the rounded lips, lips 3 and 4). Schlieren photographs for lips 2 and 3, figure 11, show characteristic shock-wave patterns. The circular patterns result from striae variations in the windows.

It should be emphasized that the experimental net drag coefficients presented include the pressure and skin-friction forces on the inlet-fuselage forebody and the cylindrical afterbody forward of the seal plus any pre-entry drag force due to changes in total momentum of the air from the free stream to the nose-inlet entrance.

## DISCUSSION

## Pressure Recovery

In general, the pressure-recovery data show that blunting the lips of the inlet increases the pressure recovery at all the speeds tested. At the take-off condition ( $M_0 = 0$ , fig. 6), there were large beneficial effects on pressure recovery and maximum mass flow of progressive increases in lip bluntness. At high subsonic and at low supersonic speeds, for  $\alpha = 0^\circ$ , figure 7 shows there was no significant effect of lip bluntness for mass-flow ratios less than 0.8. However, increased bluntness did increase the pressure recovery slightly at mass-flow ratios

between 0.8 and choking, except for the most blunt lip at supersonic speeds. Figure 8 indicates that the adverse effects on pressure recovery due to increases in angle of attack at subsonic speeds are not as large for lips with increasing leading-edge bluntness. This effect of lip bluntness at angle of attack is most pronounced for mass-flow ratios above 0.8.

The improvements in pressure recovery due to blunting the lip were small at supersonic and at high subsonic speeds. It should be kept in mind, however, that some slight rounding and internal contraction, such as was incorporated in lip 3, markedly improved the take-off performance and gave measurable increases in pressure recovery at all the speeds tested.

The pressure recovery at supersonic speeds, predicted by combining a normal-shock loss with a theoretical subsonic diffuser efficiency,  $\eta$ , of 0.92, shows good agreement with measured values up to mass-flow ratios of approximately 0.90 (fig. 7(f)). As the mass-flow ratio was increased from 0.9 to choking, the losses were consistently underestimated for all lip shapes at the supersonic Mach numbers investigated.

### Net Drag

Measured drag.- The net drag coefficients of the four lip models are shown as a function of mass-flow ratio in figure 9 for the supersonic test Mach numbers. These data show that considerable rounding of the lip and some internal contraction can be tolerated with almost no change in drag.

The subsonic type of lip bluntness and internal contraction, typified by lip 4, results in substantially greater drag than that obtained from the sharper lips. In the mass-flow-ratio range of primary interest (from 0.8 to maximum), there is little difference in the drag characteristics between lips 1, 2, and 3. Several of the curves shown in figure 9 exhibited an inflection at mass-flow ratios near maximum which cannot be explained by the evidence available. Figures 10(a) and 10(b), which are typical of the sharp and blunt lips, show that the change in drag coefficient with angles of attack up to  $5^\circ$  is small.

Comparison of measured and estimated drag.- The drag considerations in Appendix A show the general expression for pre-entry drag at both subsonic and supersonic speeds to be as follows:

$$D_{pe} = \int_0^{\text{stagnation}} (p - p_o) dA$$

At subsonic speeds, provided there is no external flow separation or shock wave, the total external net drag remains unchanged with decreasing mass-flow ratio because the pre-entry drag is compensated by an equal and opposite change in body pressure drag in the region of the inlet lip. The variation of net drag with mass-flow ratio at supersonic speed may be considered to be equal to the pre-entry drag if no allowance is made for lip suction forces (refs. 3, 9, and 10). Fraenkel, reference 11, puts forth the idea, however, that suction forces do exist at supersonic speeds similar to those at subsonic speeds, but to a lesser degree. It is reasoned that although it is impossible to attain a lip suction force exactly equal to the pre-entry drag at supersonic speeds because of normal-shock-wave losses, the inlet is operating in a subsonic flow field, and a lip suction force that neutralizes at least a portion of the pre-entry drag should be present.<sup>1</sup> The two assumptions used in predicting the net drag variation, (1) no leading-edge suction, and (2) full leading-edge suction, are compared to the experimental drag of lips 1 and 4 in figure 12. Since the theory gives only a variation of drag with mass-flow ratio, the theoretical drag curves are adjusted to the experimental curves at the maximum mass-flow ratio. The mass-flow ratios of figure 12 are based on the lip leading-edge area to give maximum accuracy as suggested in Appendix A. It should be remembered that

$$\frac{m_{le}}{m_0} = \frac{m_1}{m_0} \frac{A_1}{A_{le}}$$

It is important to note that the variation of net drag for lip 4 is predicted quite closely by allowing for the possible lip suction. Figure 12 also shows that lip shape had little effect on the magnitude of the lip suction forces. In the range of mass-flow ratios from 0.8 to a maximum, very little lip suction force is available and the drag curve is predicted by either method. As mass-flow ratio is decreased, allowance for the relatively large lip suction force becomes necessary.

Since it is possible to establish the general slope of the net drag curve, it is only necessary to calculate the level of minimum drag at the maximum mass-flow ratio for prediction of the drag curve. The minimum net drag includes components of pressure drag, drag due to friction, and, in many cases, pre-entry drag brought about by internal contraction which causes subcritical operation of the inlet. For the sharp-lip case, all three of these components may be estimated with considerable accuracy (refs. 9, 11, 12, and 13). When round lips are used, the friction drag

<sup>1</sup>The suction force, according to reference 11, may be calculated as follows: If  $p_0'$  denotes the static pressure following the shock wave, then

$$\Delta D = \int_0^{\text{stagnation}} (p - p_0') dA$$

and pre-entry drag can be estimated; however, an accurate method for calculating the pressure drag is unavailable.

### Analysis

To compare these individual lip shapes requires that their internal characteristics (pressure recovery) be related to an appropriate engine, and that their external characteristics (drag) be related to an assumed airplane. The J-57 jet engine has been chosen, and a wing area of 376 square feet has been assumed for the airplane. The performance comparison of the lip shapes is made by combining the drag force and the pressure recovery into a single parameter. In this analysis, the loss

in pressure recovery  $\left( \text{i.e., } 1 - \frac{p_{tc}}{p_{t0}} \right)$  is converted to a thrust loss

through use of a value of 1.21 for the factor  $\frac{\Delta F/F_{isen}}{\Delta p_t/p_{t0}}$ , this value being

appropriate for the J-57 jet engine for the assumed flight conditions. This thrust loss is then combined with the drag to give an effective drag coefficient based on wing area.

The inlets must also be compared at their actual operating points. At the operating (or "matched") condition, the air supplied by the inlet must be equal to the air required by the engine. The operating mass-flow ratios and the corresponding pressure recovery and drag coefficients were obtained for each inlet at several assumed inlet areas. The method used is outlined in Appendix B, and typical curves for one lip shape are given in figure 13. It should be mentioned that as the inlet area is reduced, the body pressure drag is increased slightly and the pre-entry drag is decreased. These effects on the drag are not included; but for the range of inlet areas of the analysis ( $A_{inlet} = 520$  to  $640$  sq in.), a study of the body pressure forces by the method of reference 9 and consideration of the pre-entry drag show these force changes to be negligible, and also of opposite sign. The results of the analysis at supersonic speeds are given for each lip in terms of an effective drag coefficient based on wing area (figs. 14 and 15).

From figure 14 it can be seen that a subsonic lip shape (lip 4) results in a considerable effective drag penalty at supersonic Mach numbers. Rounding of the lip and some internal contraction (lip 3) is beneficial. Because there is only a small variation in  $C_D$  with inlet area for most of the lip shapes, it can be said that the performance of the inlets is not sensitive to changes in inlet area from 540 to 640 square inches. In figure 13 it is shown that an inlet area of 540 square inches requires a mass-flow ratio of approximately 0.92 at all Mach

numbers, and that an air inlet area of 640 square inches requires a mass-flow ratio of 0.8. By substitution of mass-flow ratio for inlet area, it can be seen that for these nose inlets it is possible to operate efficiently with a fixed-area inlet over a range of mass-flow ratios, and thus reduce considerably the problem of engine-inlet optimization.

The effect of free-stream Mach number on the effective drag coefficient of the inlet-fuselage combination, for two inlet areas, is shown in figure 15. It can be observed that  $C_D'$  increases more rapidly with Mach number than does the basic body from which the inlet-fuselage was derived. This effective drag increase is caused mainly by the thrust loss resulting from the loss of pressure recovery of the normal-shock inlets. At Mach numbers greater than about 1.35, a pressure recovery above that for a normal shock could reduce the magnitude of this drag increase.

The variation of pressure recovery for the four lip shapes with Mach number, for the operating conditions of the inlet-engine combination, is shown in figure 16. Two inlet areas, 540 and 640 square inches, are presented. A considerable improvement in pressure recovery at subsonic speeds results when the larger inlet area (640 sq in.) is used. Figures 14 and 15 also indicate no increase in  $C_D'$  for the 640-square-inch inlet area at  $M = 1.23$ .

### CONCLUSIONS

The following conclusions were obtained from an investigation of the effect of lip shape on the performance of a nose-inlet air-induction system.

1. Rounding the lip had a favorable effect on total pressure recovery over the range of test Mach numbers from 0 to 1.50. The pressure-recovery differences were generally small, with the exception of the take-off condition where rounding the lip gave considerable increase in pressure recovery.

2. At supersonic Mach numbers the net drag at mass-flow ratios from 0.80 to the maximum was essentially unchanged by moderate rounding of the lip. Excessive lip rounding, however, resulted in considerable drag increase at all mass-flow ratios.

3. The increase in drag coefficient with decreasing mass-flow ratio at supersonic speeds can be predicted by allowing for cowl leading-edge suction as suggested by Fraenkel.

4. A comparison of the four lip shapes based on an effective drag coefficient over a range of supersonic Mach numbers up to 1.50 shows that some lip roundness and internal contraction is beneficial.

5. Normal-shock nose inlets in combination with a J-57 engine can operate efficiently over a sufficient range of mass-flow ratios to permit use of a fixed-area inlet up to a Mach number of 1.50.

Ames Aeronautical Laboratory  
National Advisory Committee for Aeronautics  
Moffett Field, Calif., Feb. 8, 1954

~~CONFIDENTIAL~~

## APPENDIX A

PRE-ENTRY DRAG CONSIDERATIONS FOR INLETS WITH ROUNDED  
LIP SHAPES

The drag components of ducted bodies have been discussed in references 6, 10, 14, and 15. Although adequate, in most cases, these analyses do not consider certain aspects of the flow field in the vicinity of the inlet lip. References 10, 14, and 15 show that

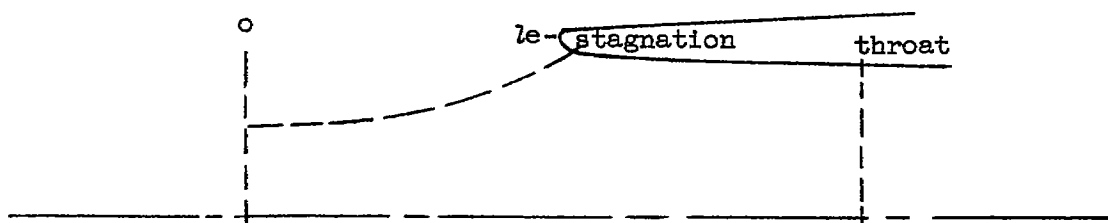
$$C_{D_{pe}} = \int_0^{\text{stagnation}} \frac{p - p_0}{q_0 A_s} dA = \frac{m(V_s - V_0) + A_s(p_s - p_0)}{q_0 A_s} \quad (A1)$$

$$C_{D_{pe}} = \left(1 - \frac{m_s}{m_0}\right)^2 \quad \text{incompressible} \quad (A2)$$

$$C_{D_{pe}} = C_{p_s} - 2 \frac{m_s}{m_0} \left(1 - \frac{V_s}{V_0}\right) \quad \text{compressible} \quad (A3)$$

It should be noted that to compute accurately the pre-entry (or additive) drag it is necessary to locate on the lip the position of the stagnation streamline. The special case generally treated is for a sharp lip, where the stagnation points for mass flows between 0 and 1.0 occur on a surface parallel to the free-stream direction.

When a rounded lip is used, the stagnation point occurs on the curved lip surface, and its location usually is not known. For this case the minimum area (throat) section and the lip leading edge can generally be assumed as the limiting locations of the stagnation point. (See sketch below.)



The pre-entry drag can be computed for either of these assumed locations of the stagnation point. If the stagnation point is assumed to be at the throat and the area,  $A_s$ , in equation (A1) is taken as  $A_{throat}$ , the calculated additive drag will be in error by the change in total momentum from the stagnation point to the throat or

$$\Delta C_{D_{pe}} \text{ (error)} = \int_{\text{stagnation}}^{\text{throat}} \frac{p - p_0}{q_0 A_{throat}} dA$$

Increasing the value of mass-flow ratio displaces the stagnation point toward the leading edge which increases the error. Mass-flow ratios near the maximum (where the error is greatest) can give negative values of  $C_{D_{pe}}$  if the minimum area station is used (ref. 14). If the stagnation point is assumed to be at the leading edge, the error would be as follows:

$$\Delta C_{D_{pe}} \text{ (error)} = \int_{\text{stagnation}}^{\text{leading edge}} \frac{p - p_0}{q_0 A_{le}} dA$$

Since the stagnation point moves inward with decreasing mass-flow ratio, the error would be greatest at  $m_{le}/m_0 = 0$ , but would be eliminated completely at a mass-flow ratio of unity ( $m_{le}/m_0 = 1.0$ ). Since the mass-flow-ratio range of interest is about 1.0, the assumptions resulting in the greatest accuracy in this region should be used. For this reason the station at the leading edge was selected for the calculation and comparison of the pre-entry drag.

## APPENDIX B

METHOD FOR EVALUATING THE OPTIMUM OPERATIONAL CHARACTERISTICS  
OF A COMBINATION OF AN AIR-INDUCTION SYSTEM AND ENGINE

At the operating condition the air supplied by the inlet must be equal to the air required by the engine

$$W_{a_{inlet}} = W_{a_{engine}} \quad (B1)$$

and

$$W_{a_{inlet}} = g \rho_o V_o A_o = g \rho_o M_o a_o A_1 \left( \frac{A_o}{A_1} \right) = g A_1 M_o \rho_o a_o \left( \frac{m_1}{m_o} \right) \quad (B2)$$

$$W_{a_{engine}} = g \rho_c V_c A_c = g \rho_c M_c a_c A_c \quad (B3)$$

The air-flow performance of a jet engine usually is expressed in terms of a "corrected" parameter. The weight of air required by the engine is referred to standard sea-level conditions.

$$W_{a_c} = g \rho_c M_c a_c A_c \left( \frac{\rho_{std}}{\rho_c} \frac{a_{std}}{a_c} \right)$$

where

$$\frac{\rho_{std}}{\rho_c} = \frac{p_{std}/T_{std}}{p_{t_c}/T_{t_c}}$$

and

$$\frac{a_{std}}{a} = \left( \frac{T_{std}}{T_{t_c}} \right)^{1/2}$$

or

$$W_{a_c} = g \rho_c M_c a_c A_c \frac{\sqrt{T_{t_c}/T_{std}}}{p_{t_c}/p_{std}} = W_{a_{(engine \text{ or } inlet)}} \frac{\sqrt{\theta}}{\delta} \quad (B4)$$

~~CONFIDENTIAL~~

Other derivations of the corrected air flow are described in references 16 and 17. Generalization of the air flow by use of this parameter permits results of specific tests of an engine to be used for estimating performance at other conditions. The factor  $\sqrt{\theta}/\delta$  can be written:

$$\frac{\sqrt{\theta}}{\delta} = \frac{\sqrt{\theta}}{\delta_{isen}} \frac{\delta_{isen}}{\delta} = \frac{\sqrt{T_{tc}/T_{std}}}{p_{t_o}/p_{std}} \frac{p_{t_o}/p_{std}}{p_{tc}/p_{std}} = \frac{\sqrt{\theta}}{\delta_{isen}} \frac{p_{t_o}}{p_{tc}}$$

where

$$\delta_{isen} = \frac{p_{t_o}}{p_{std}}$$

Referring now to the flow through the inlet, equation (B2) becomes, through substitution

$$W_a \frac{\sqrt{\theta}}{\delta} = g A_1 M_o \rho_o a_o \left( \frac{m_1}{m_o} \right) \frac{\sqrt{\theta}}{\delta_{isen}} \frac{p_{t_o}}{p_{tc}}$$

and

$$\frac{W_a}{A_1} \frac{\sqrt{\theta}}{\delta} \left( \frac{p_{tc}}{p_{t_o}} \right) = g M_o \rho_o a_o \left( \frac{m_1}{m_o} \right) \frac{\sqrt{\theta}}{\delta_{isen}} = 85.4 \frac{m_1}{m_o} \left[ \frac{M_o}{(1 + 0.2 M_o^2)^3} \right]$$

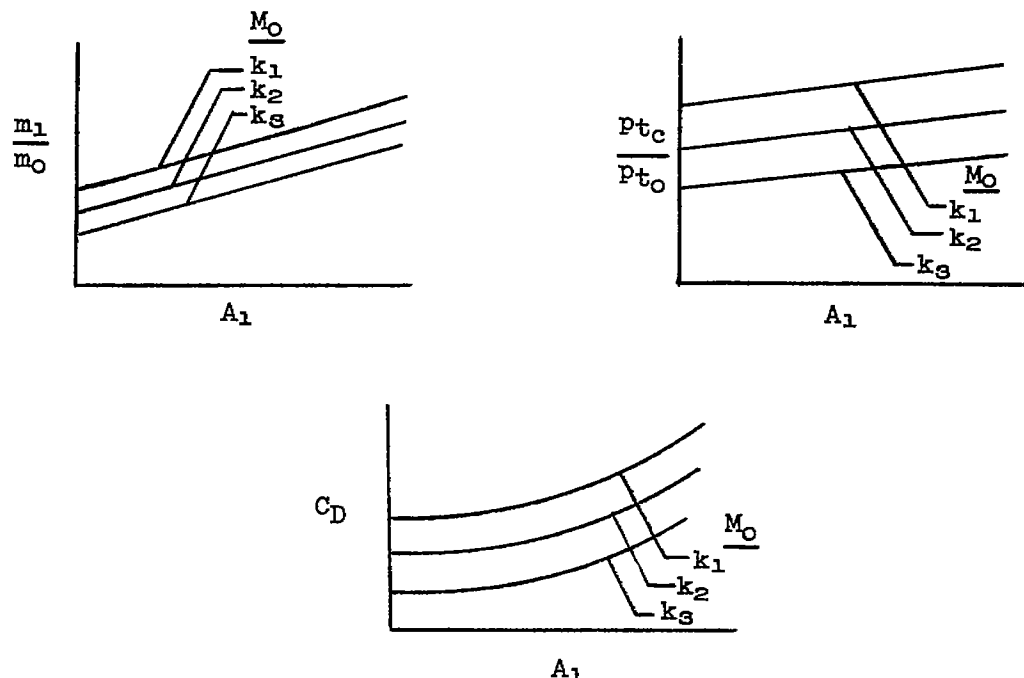
where

$$\begin{aligned} g &= 32.17 \text{ ft/sec}^2 \\ \rho_o &= 0.002376 \text{ slugs/ft}^3 \\ a_o &= 1117 \text{ ft/sec} \end{aligned}$$

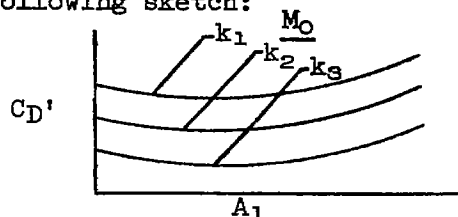
It should be noted that the right side of the equation for "generalized inlet-engine" parameter  $\left( \frac{W_a}{A_1} \frac{\sqrt{\theta}}{\delta} \frac{p_{tc}}{p_{t_o}} \right)$  is a function only of  $M_o$  and  $m_1/m_o$  and is independent of altitude.

This generalized inlet-engine parameter can be used as the link for relating the air supplied by the inlet at a given pressure recovery ( $p_{t_c}/p_{t_o}$ ) to the air required by the engine. The solution is graphical and is illustrated in figure 17. The choking limit shown on the upper right-hand quadrant is that imposed by aerodynamic considerations of the maximum flow possible through a given inlet area.

The actual operating  $m_1/m_o$ ,  $p_{t_c}/p_{t_o}$ , and  $C_D$  can be obtained as a function of inlet area. Examples obtained by this graphical solution are sketched below (see also fig. 13):



The optimum operation of the inlet-engine combination is then computed by converting the loss in pressure recovery (i.e.,  $1 - p_{t_c}/p_{t_o}$ ) to a thrust loss, and then combining this thrust loss with the measured drag to give an effective-drag coefficient as a function of inlet area, illustrated in the following sketch:

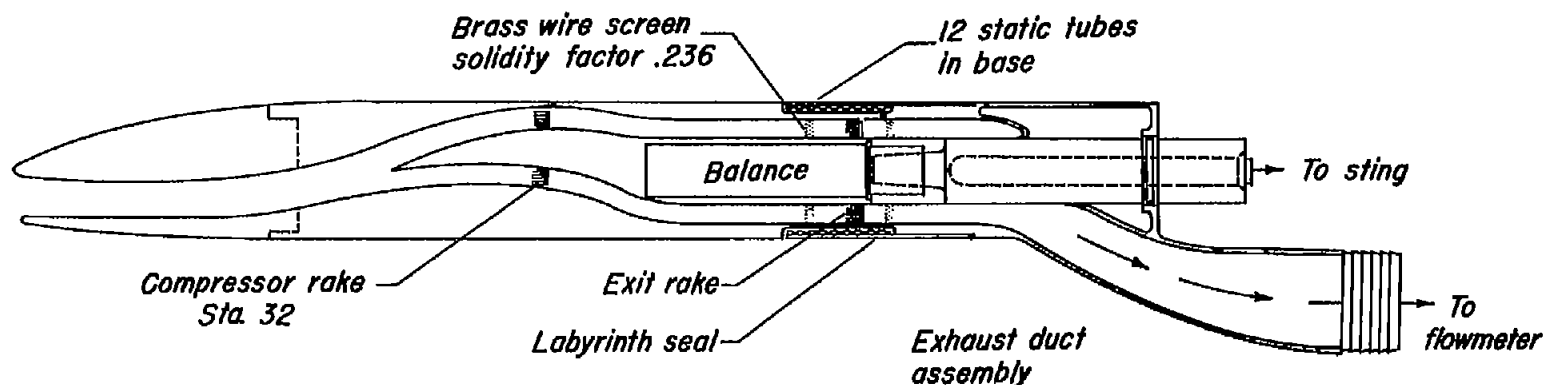


The optimum operating point or the optimum operating range of the engine-inlet combination can then be selected.

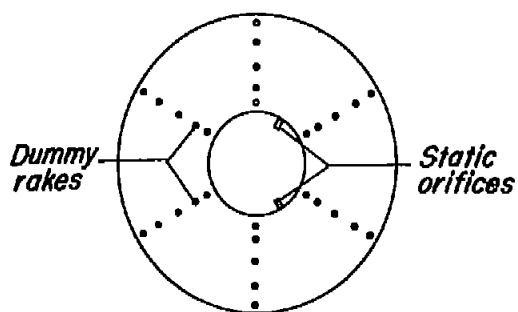
## REFERENCES

1. Baals, Donald D., Smith, Norman F., and Wright, John B.: The Development and Application of High-Critical-Speed Nose Inlets. NACA Rep. 920, 1948.
2. Seddon, J.: Air Intakes for Aircraft Gas Turbines. Jour. Roy. Aero. Soc., Oct. 1952.
3. Ferri, Antonio, Nucci, Louis M.: Preliminary Investigation of a New Type of Supersonic Inlet. NACA TN 2286, 1951.
4. Cortright, Edgar M., Jr., and Connors, James F.: Survey of Some Preliminary Investigations of Supersonic Diffusers at High Mach Numbers. NACA RM E52E20, 1952.
5. Weinstein, M. I.: Performance of Supersonic Scoop Inlets. NACA RM E52A22, 1952.
6. Pendley, Robert E., Milillo, Joseph R., and Fleming, Frank F.: An Investigation of Three NACA 1-Series Nose Inlets at Subsonic and Transonic Speeds. NACA RM L52J23, 1953.
7. Sears, R. I., Merlet, C. F., and Putland, L. W.: Flight Determination of Drag of Normal-Shock Nose Inlets with Various Cowling Profiles at Mach Numbers from 0.9 to 1.5. NACA RM L53I25a, 1953.
8. Frick, Charles W., and Olson Robert N.: Flow Studies in the Asymmetric Adjustable Nozzle of the Ames 6- by 6-Foot Supersonic Wind Tunnel. NACA RM A9E24, 1949.
9. Brajnikoff, George B., and Rogers, Arthur W.: Characteristics of Four Nose Inlets as Measured at Mach Numbers Between 1.4 and 2.0. NACA RM A51C12, 1951.
10. Sibulkin, Merwin: Theoretical and Experimental Investigation of Additive Drag. NACA RM E51B13, 1951.
11. Fraenkel, L. E.: The External Drag of Some Pitot-Type Intakes at Supersonic Speeds: Part I. R.A.E. Rep. Aero. 2380, June 1950.
12. Jack, John R.: Theoretical Wave Drags and Pressure Distributions for Axially Symmetric Open-Nose Bodies. NACA TN 2115, 1950.
13. Van Dyke, Milton D.: A Study of Second-Order Supersonic Flow Theory. NACA Rep. 1081, 1952.

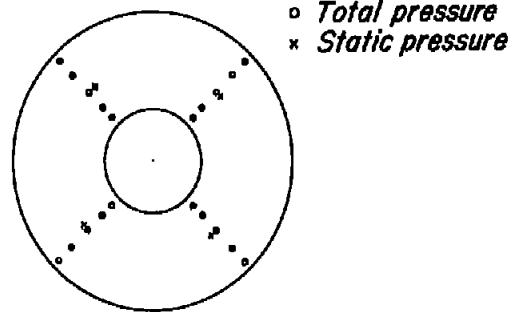
14. Klein, Harold: The Calculation of the Scoop Drag for a General Configuration in a Supersonic Stream. Douglas Aircraft Co. Rep. SM-13744, Apr. 1950.
15. Coale, Charles W.: Suction Force on the Lip of a Two-Dimensional Idealized Scoop in Non-Viscous Subsonic Flow. Douglas Aircraft Co. Rep. SM-13742, Apr. 1950.
16. Auyer, E. L., and Warner, Donald F.: Basis of Correction of Test Results and Extrapolation to Altitude Conditions for Type I Jet-Propulsion Aircraft Gas Turbines. General Electric Co. Bull. D. F. 81407, Oct. 1945.
17. Sanders, Newell D.: Performance Parameters for Jet-Propulsion Engines. NACA TN 1106, 1946.



Dimensions:  
Length=63.75 in.  
Maximum diameter = 6.62 in.



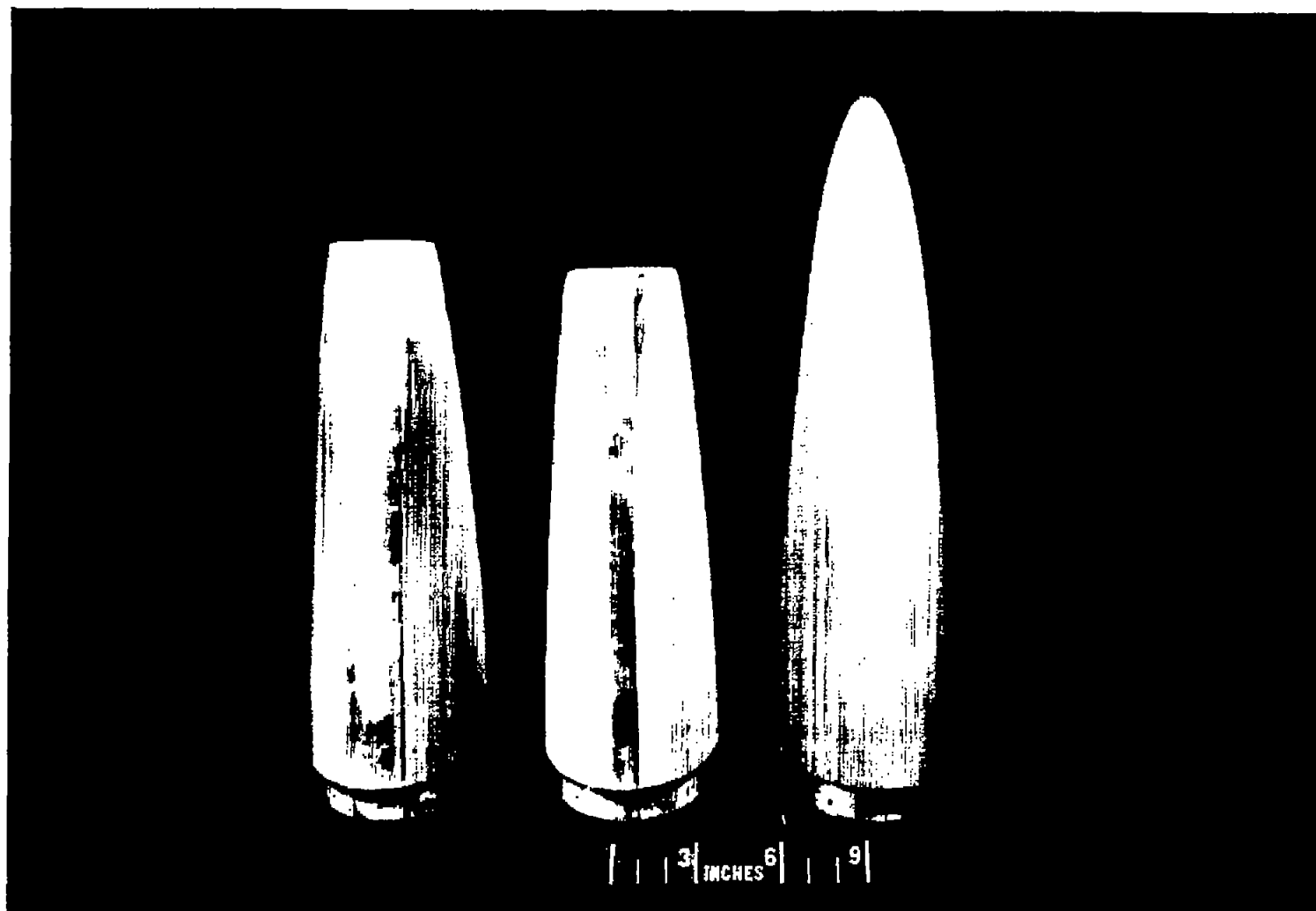
Compressor rake looking aft.



Exit rake looking aft.



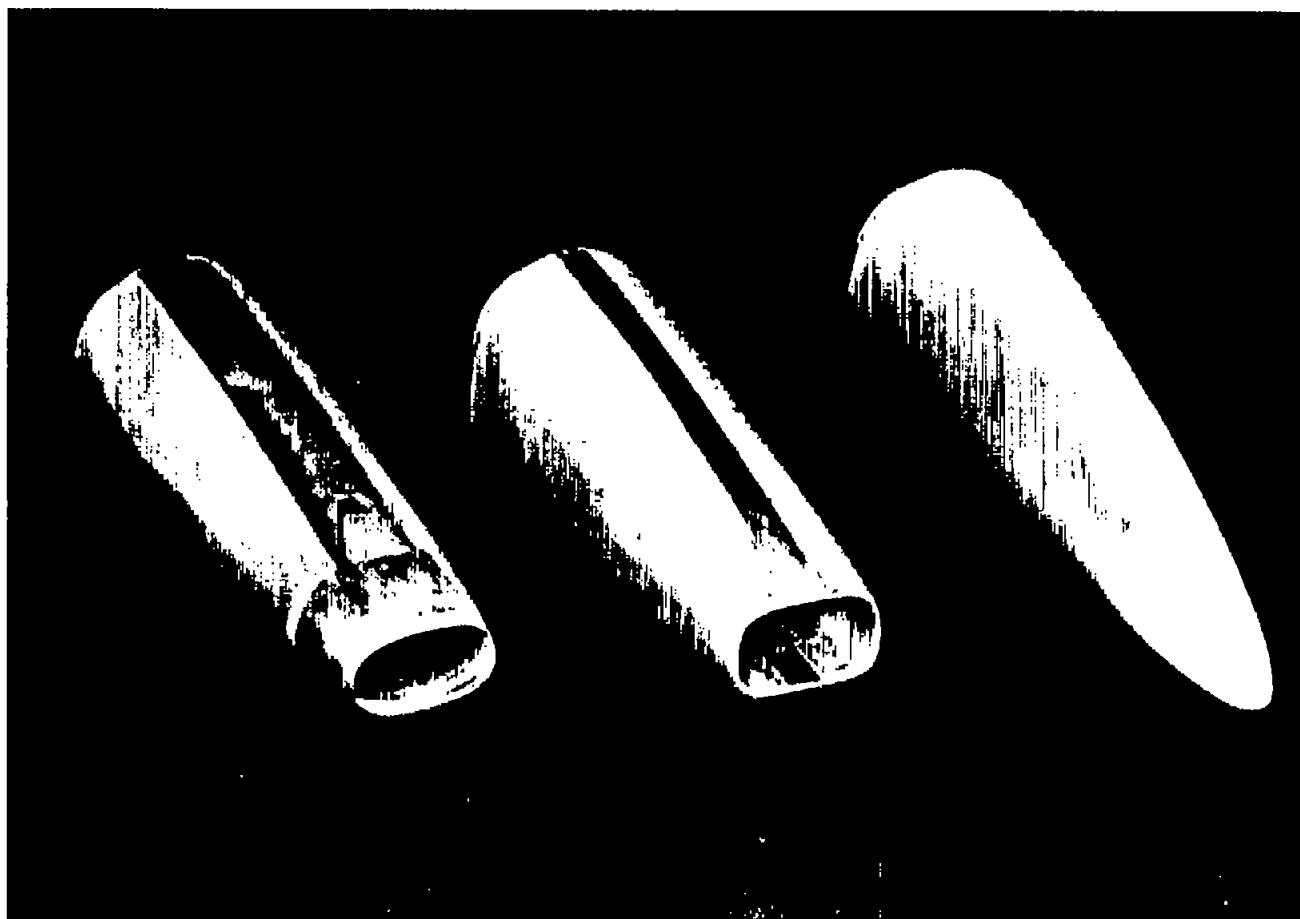
Figure 1.- Sketch of air-induction model.



(a) Top view.

A-17532.1

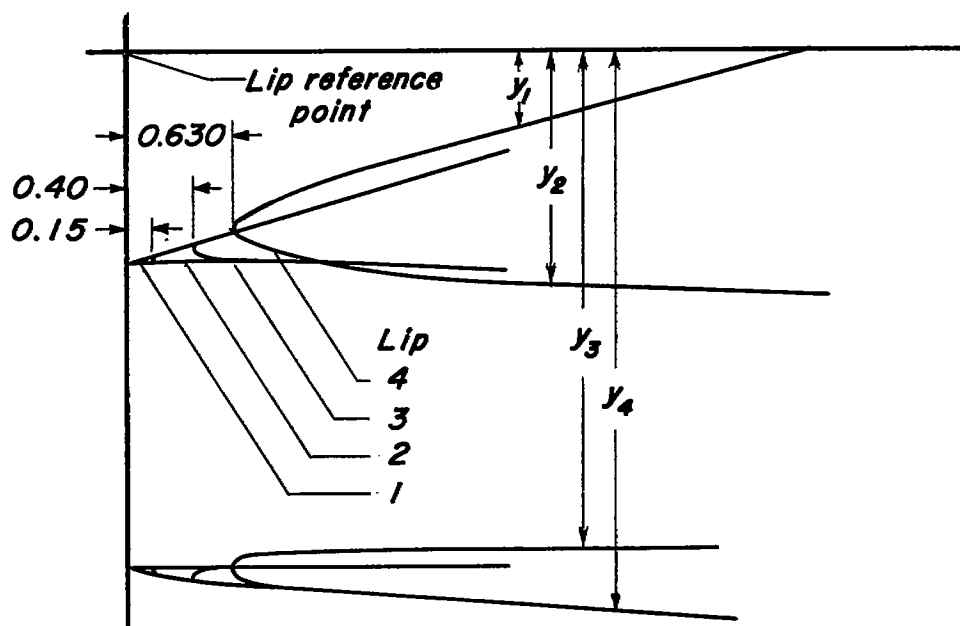
Figure 2.- Photographs of lip models 1 and 4 shown with basic body.



A-17533.1

(b) Three-quarter front view.

Figure 2.- Concluded.



<i>Lip 1</i>				
<i>Leading-edge radius = 0</i>				
<i>x</i>	<i>y<sub>1</sub></i>	<i>y<sub>2</sub></i>	<i>y<sub>3</sub></i>	<i>y<sub>4</sub></i>
0	-1.408	-1.408	-3.437	-3.437
.040	-1.396	-1.408	-3.437	-3.453
.100	-1.378	-1.408	-3.436	-3.470
.156	-1.361	-1.408	-3.435	-3.484
.203	-1.346	-1.408	-3.434	-3.495
.396	-1.286	-1.408	-3.430	-3.523
.640	-1.208	-1.408	-3.430	-3.541

<i>Lip 2</i>				
<i>Leading-edge radius = 0.025</i>				
<i>x</i>	<i>y<sub>1</sub></i>	<i>y<sub>2</sub></i>	<i>y<sub>3</sub></i>	<i>y<sub>4</sub></i>
.150	-1.382	-1.382	-3.460	-3.460
.156	-1.366	-1.399	-3.444	-3.475
.177	-1.355	-1.406	-3.436	-3.486
.203	-1.346	-1.408	-3.434	-3.495
.290	-1.319	-1.408	-3.430	-3.509
.343	-1.302	-1.408	-3.430	-3.517
.396	-1.286	-1.408	-3.430	-3.523

<i>Lip 3</i>				
<i>Leading-edge radius = 0.025</i>				
<i>x</i>	<i>y<sub>1</sub></i>	<i>y<sub>2</sub></i>	<i>y<sub>3</sub></i>	<i>y<sub>4</sub></i>
.400	-1.300	-1.300	-3.502	-3.502
.408	-1.284	-1.315	-3.482	-3.521
.430	-1.273	-1.338	-3.470	-3.526
.480	-1.257	-1.360	-3.454	-3.530
.560	-1.233	-1.376	-3.438	-3.535
.640	-1.208	-1.385	-3.430	-3.541
.800	-1.158	-1.392	-3.430	-3.553
1.200	-1.028	-1.409	-3.430	-3.580
2.300	-.683	-1.443	-3.430	-3.658

<i>Lip 4</i>				
<i>Leading-edge radius = 0.025</i>				
<i>x</i>	<i>y<sub>1</sub></i>	<i>y<sub>2</sub></i>	<i>y<sub>3</sub></i>	<i>y<sub>4</sub></i>
.630	-1.172	-1.172	-3.415	-3.415
.653	-1.143	-1.202	-3.380	-3.450
.693	-1.120	-1.223	-3.360	-3.480
.793	-1.062	-1.260	-3.335	-3.522
1.033	-.952	-1.338	-3.308	-3.562
1.333	-.839	-1.402	-3.300	-3.597
1.663	-.740	-1.450	-3.300	-3.625
2.633	-.644	-1.558	-3.300	-3.700
3.633	-.608	-1.600	-3.300	-3.759

NACA

Figure 3.- Lip coordinates.

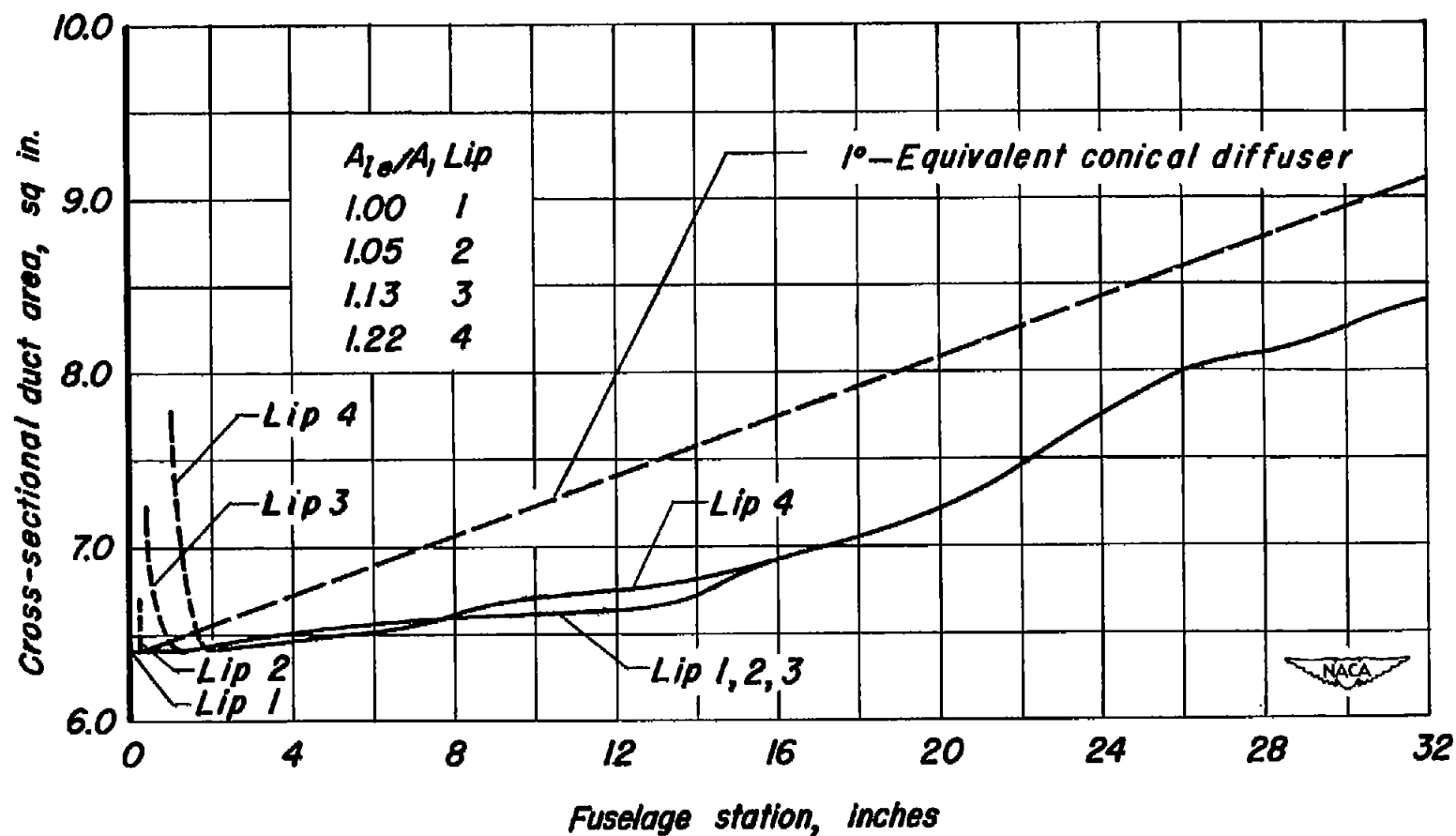


Figure 4.— Area variation in diffuser behind lip. Leading edge for the four lip models tested.



Figure 5.- Photograph of model installed in Ames 6- by 6-foot wind tunnel.

A-17569.1

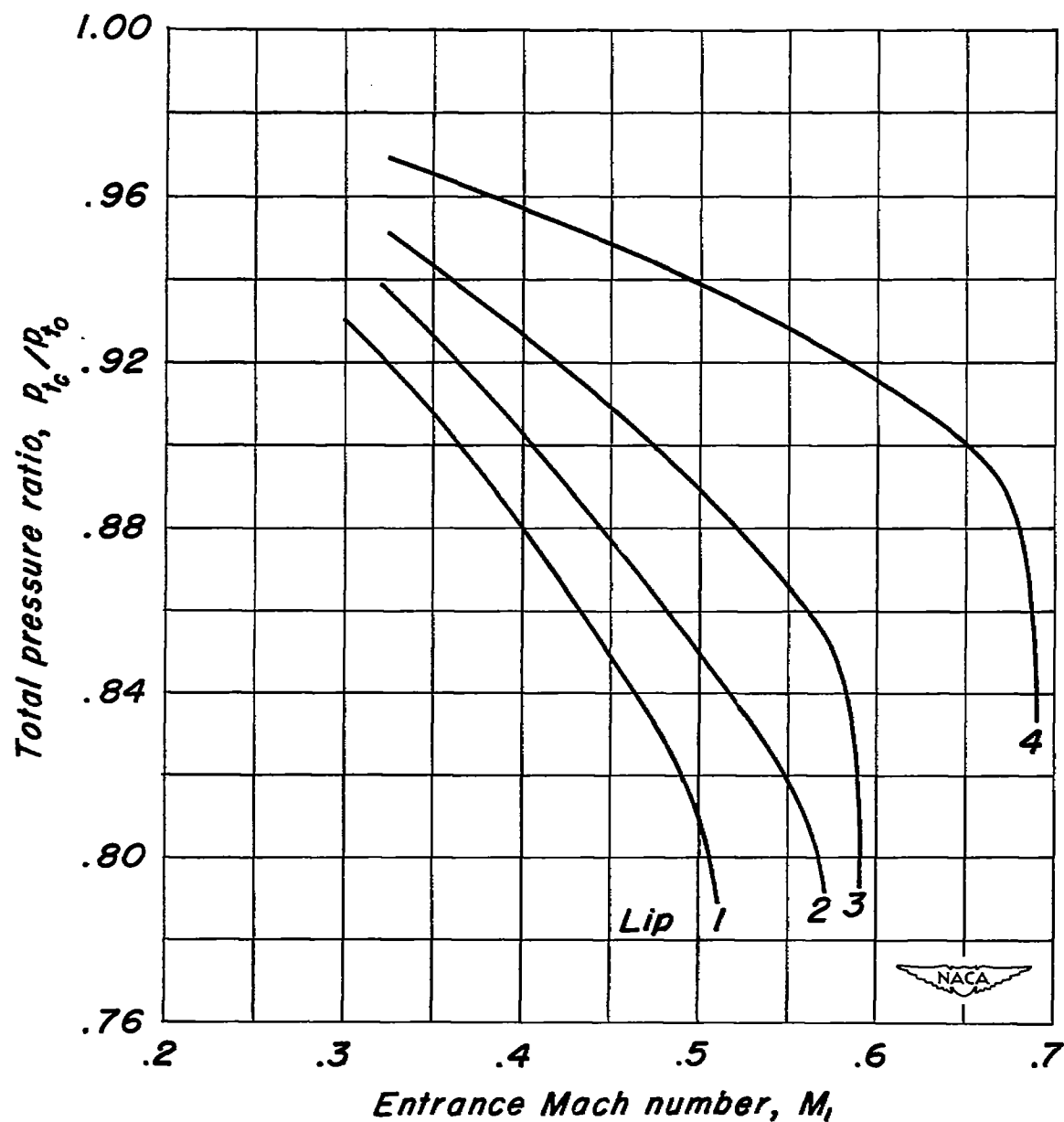
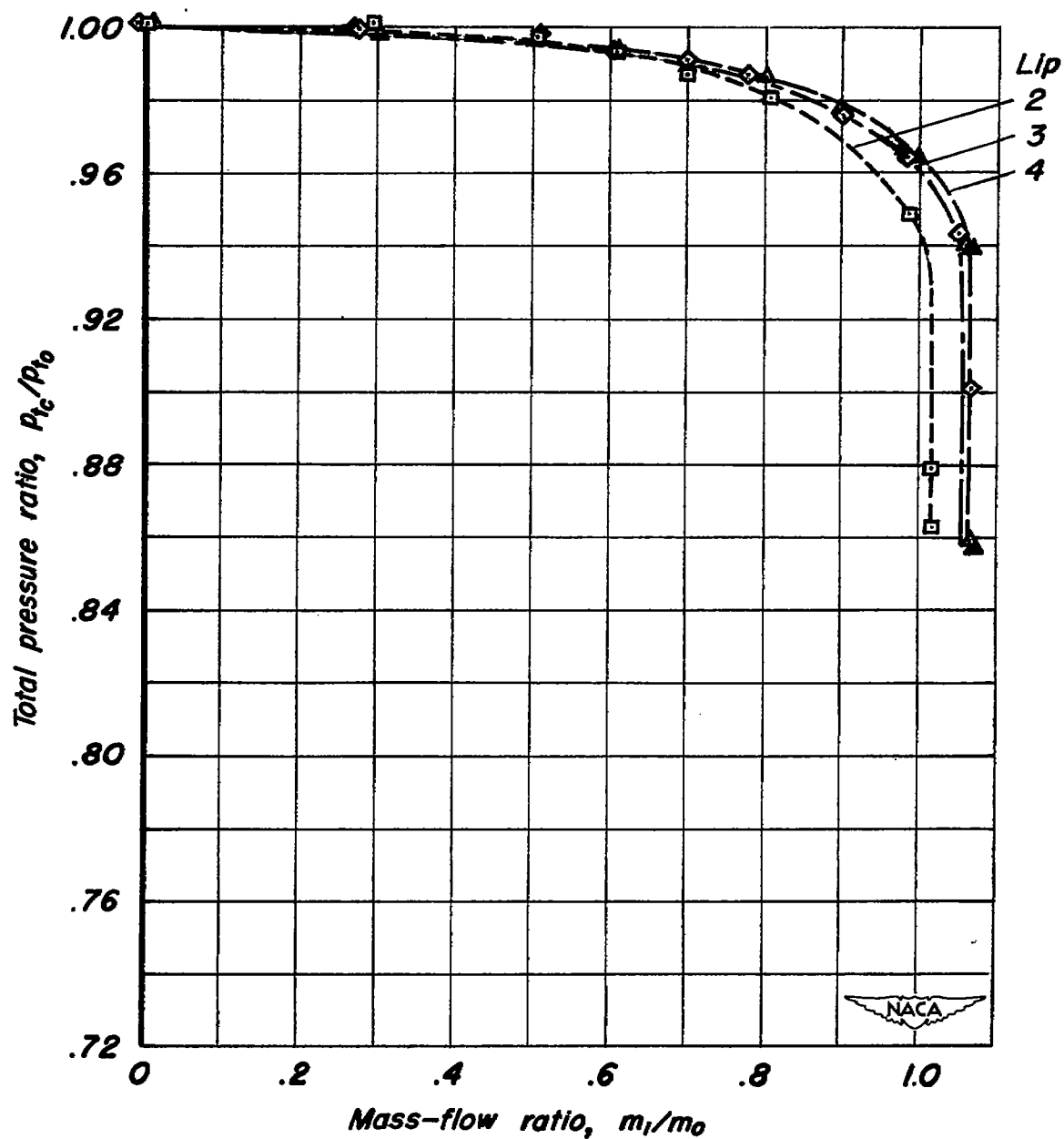
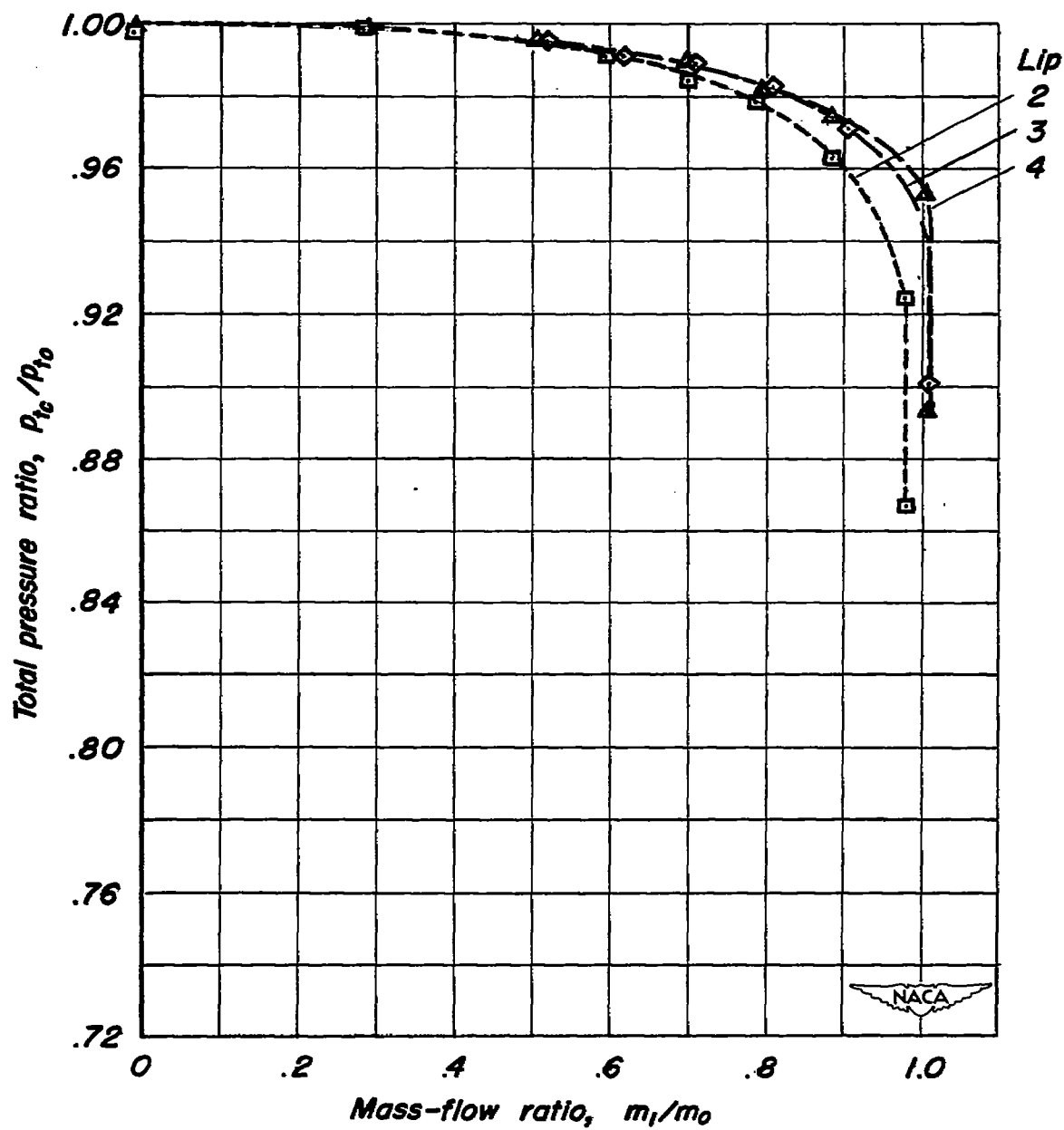


Figure 6.- The variation of pressure-recovery ratio with entrance Mach number for static operating condition ( $M_0 = 0$ ).



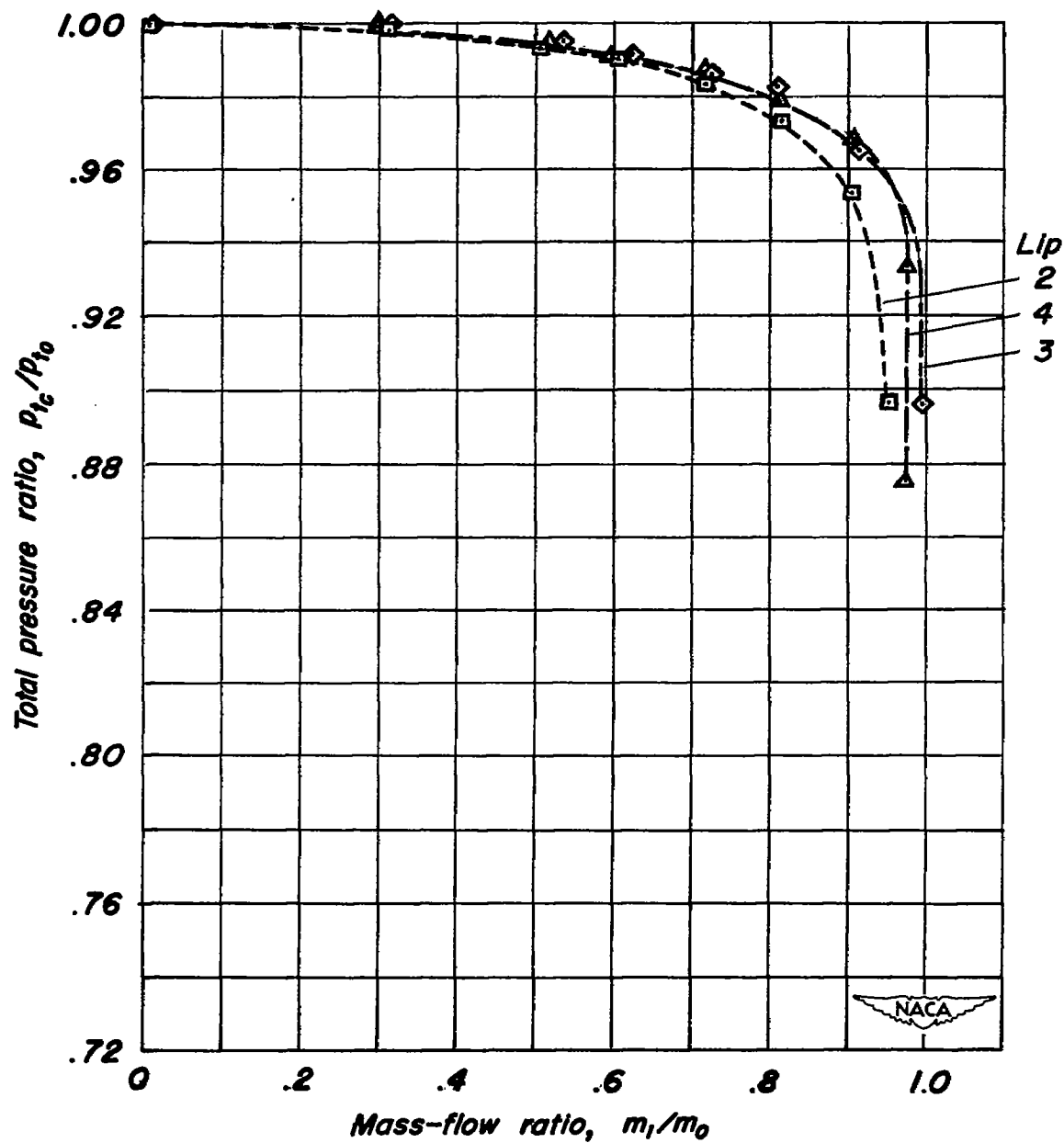
(a)  $M_0 = 0.70$

Figure 7.- The variation of pressure-recovery ratio with mass-flow ratio;  
 $\alpha = 0^\circ$



(b)  $M_0 = 0.80$

Figure 7.- Continued.



(c)  $M_0 = 0.90$

Figure 7.- Continued.

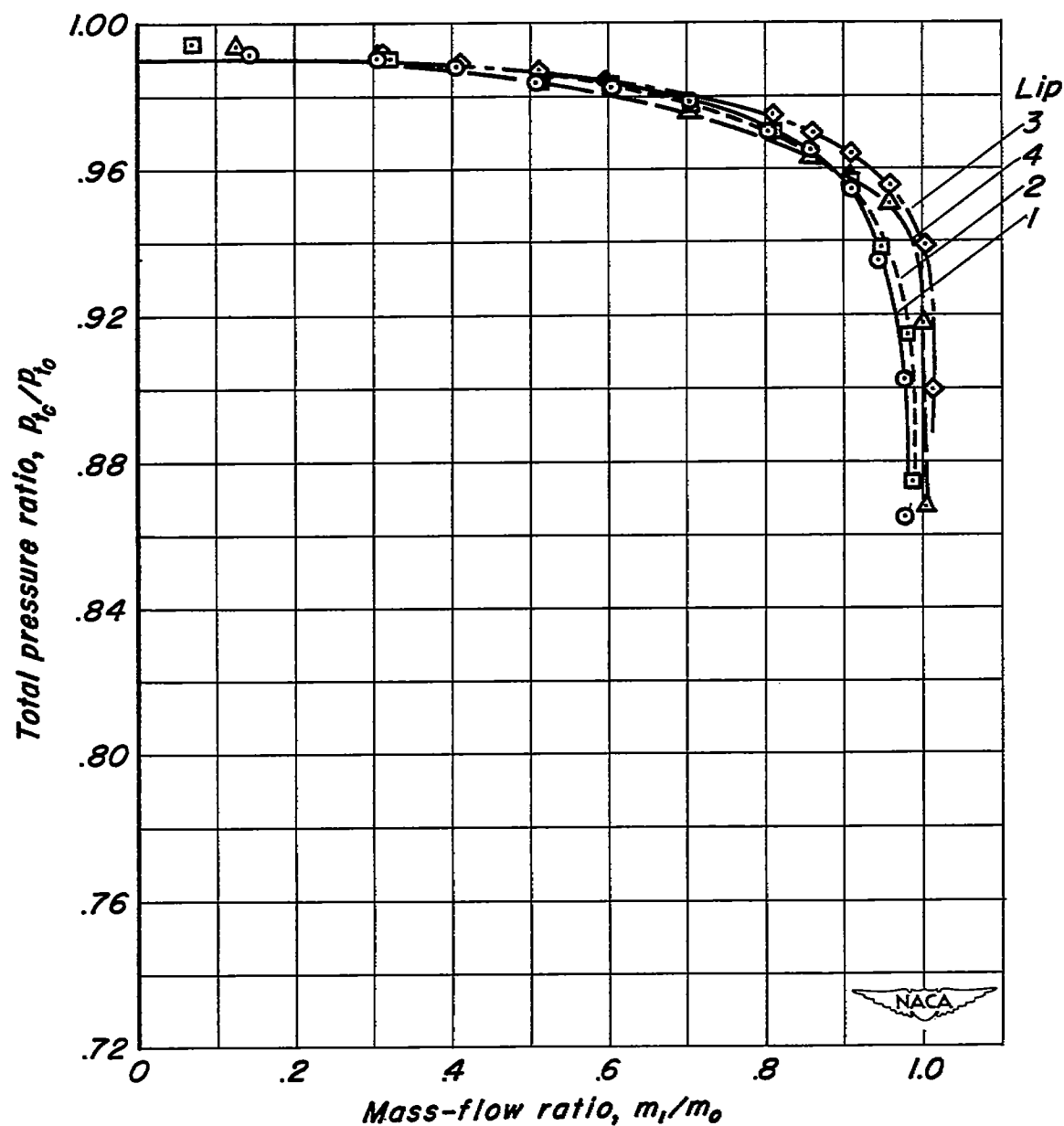
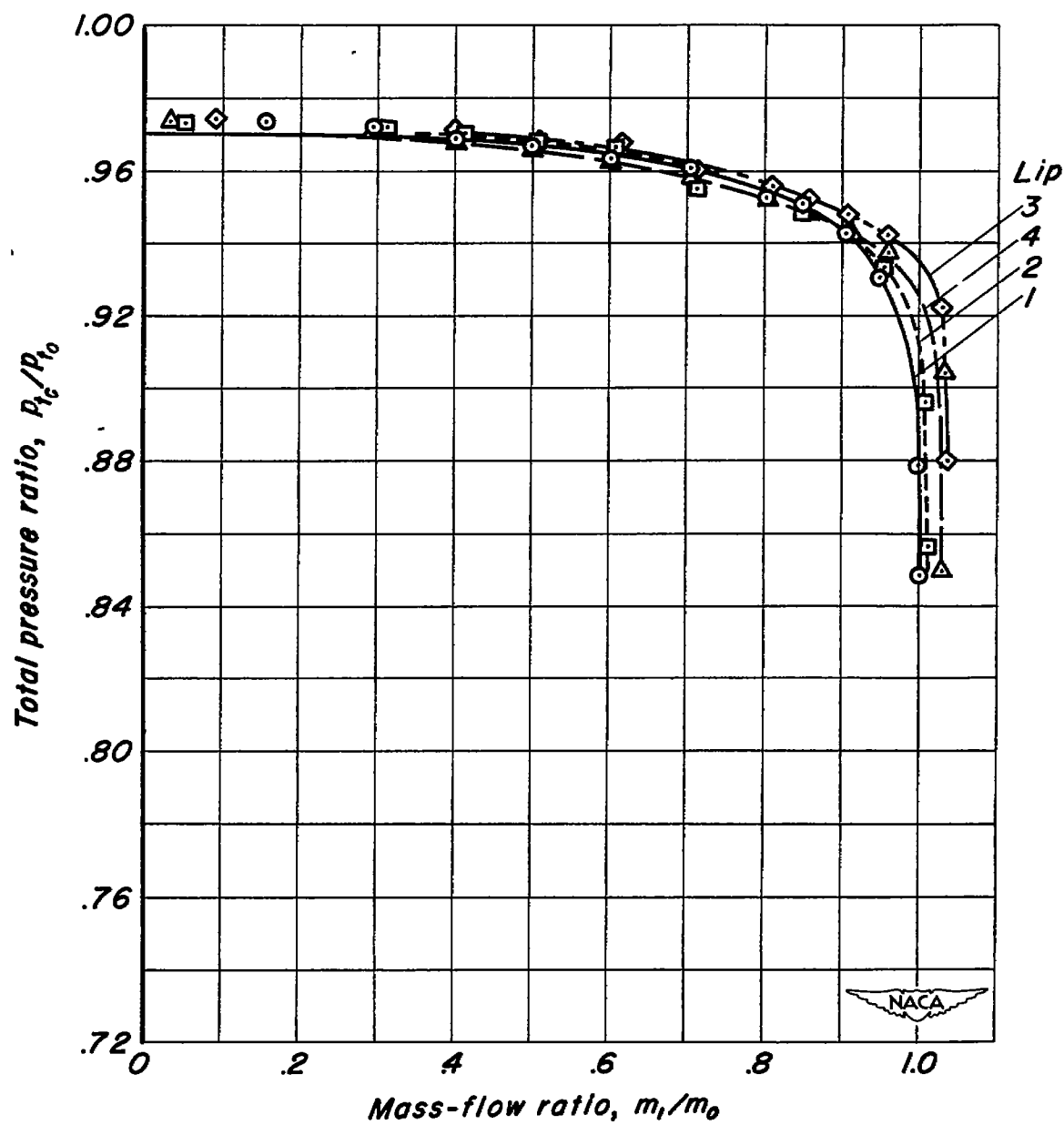
(d)  $M_0 = 1.23$ 

Figure 7.- Continued.



(e)  $M_0 = 1.35$

Figure 7.- Continued.

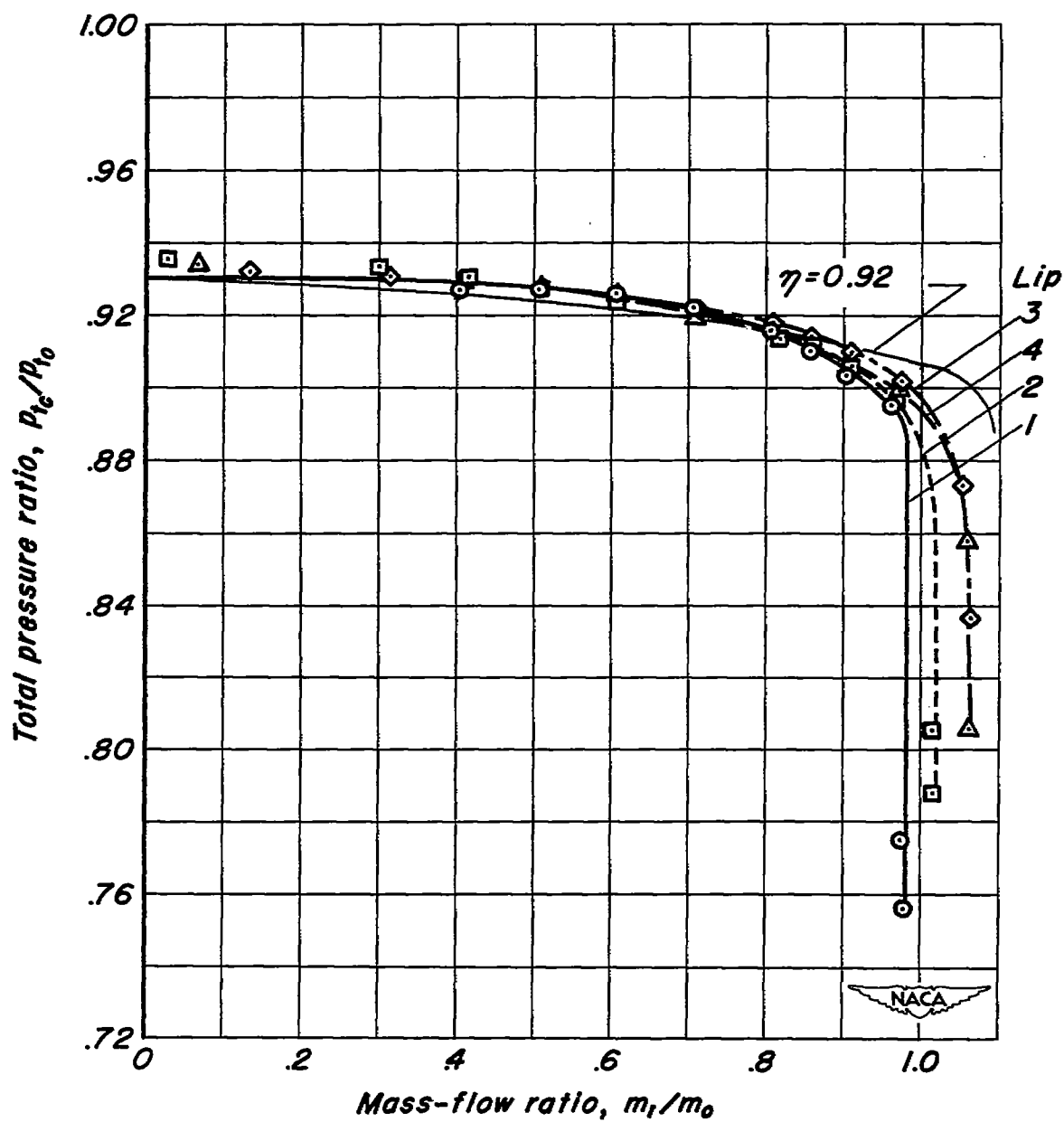
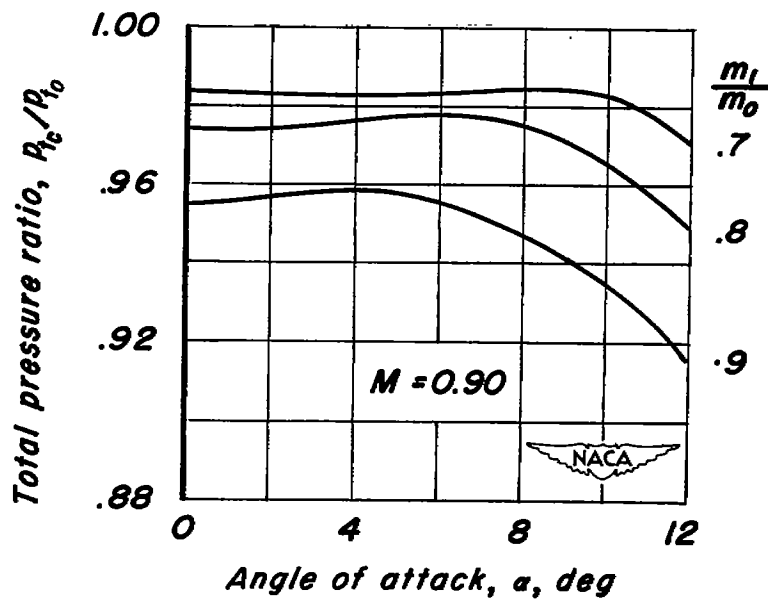
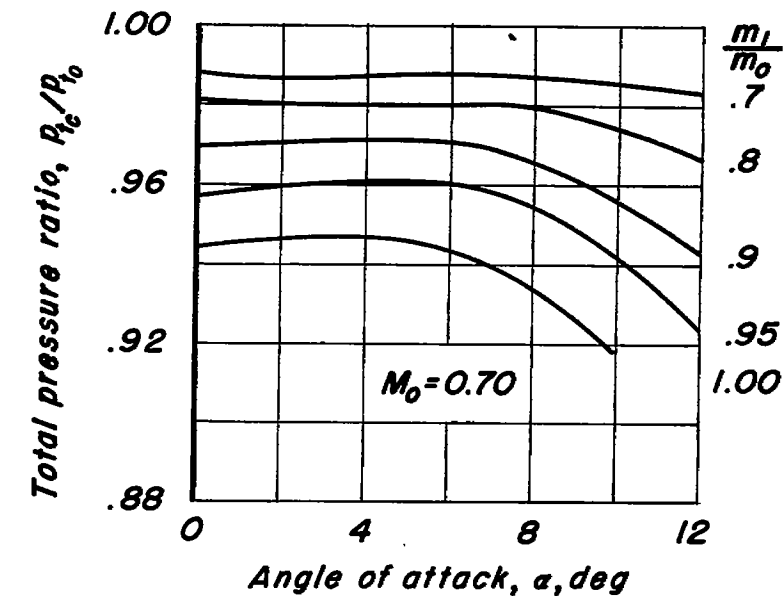
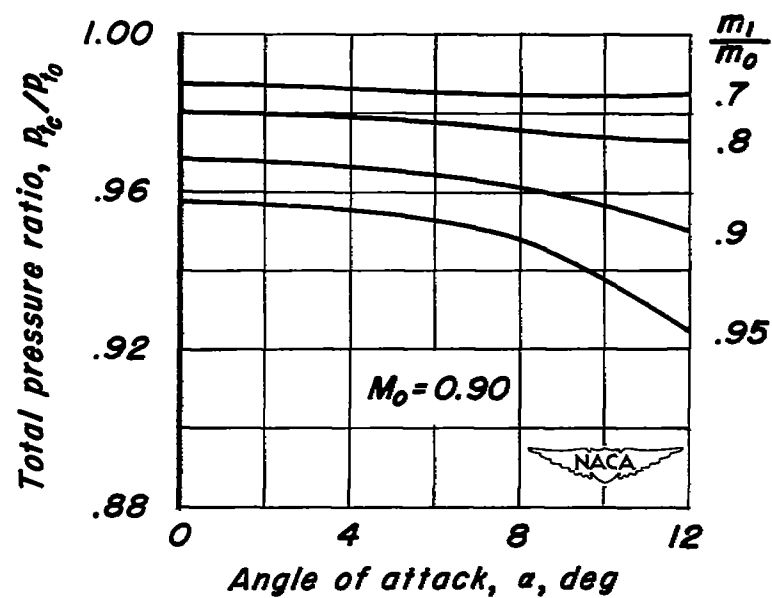
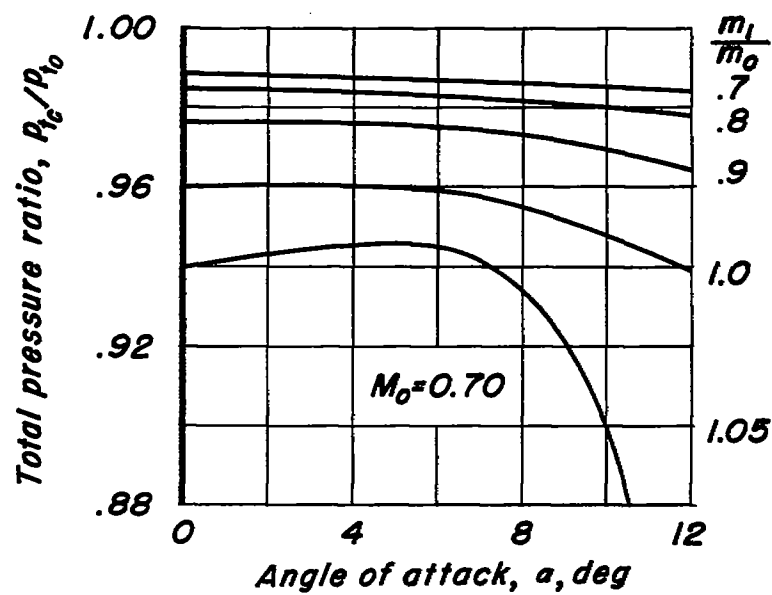
(f)  $M_0 = 1.50$ 

Figure 7.- Concluded.



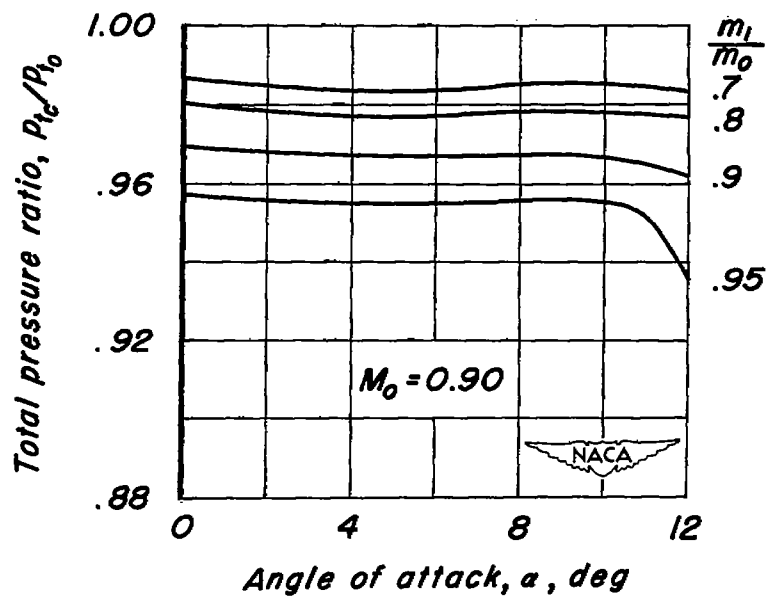
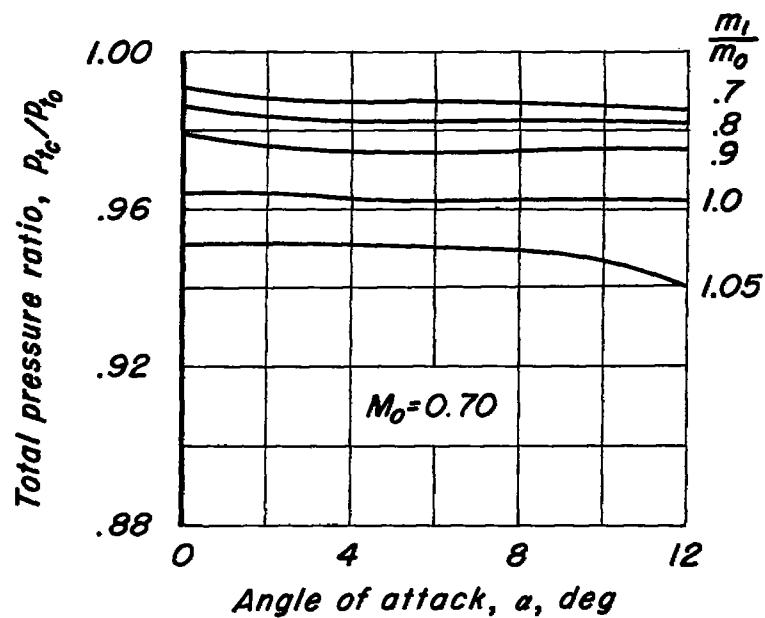
(a) Lip 2

Figure 8.- The effect of angle of attack on the pressure-recovery ratio for a range of mass-flow ratios at subsonic Mach numbers.



(b) Lip 3

Figure 8.- Continued.



(c) Lip 4

Figure 8.- Concluded.

~~CONFIDENTIAL~~

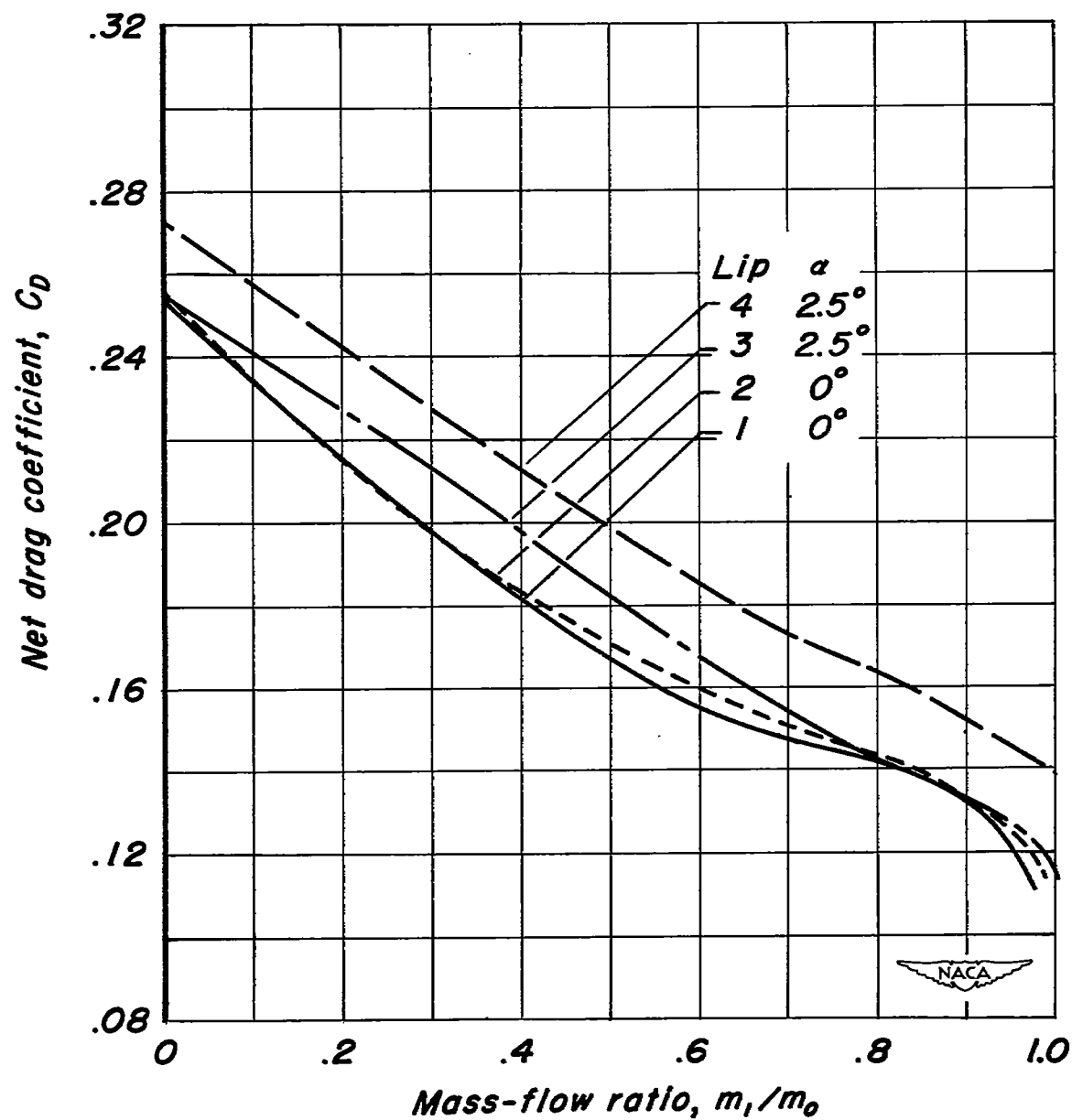
(a)  $M_0 = 1.23$ 

Figure 9.- The variation of net drag coefficient with mass-flow ratio for the angles of attack of minimum drag at supersonic Mach numbers.

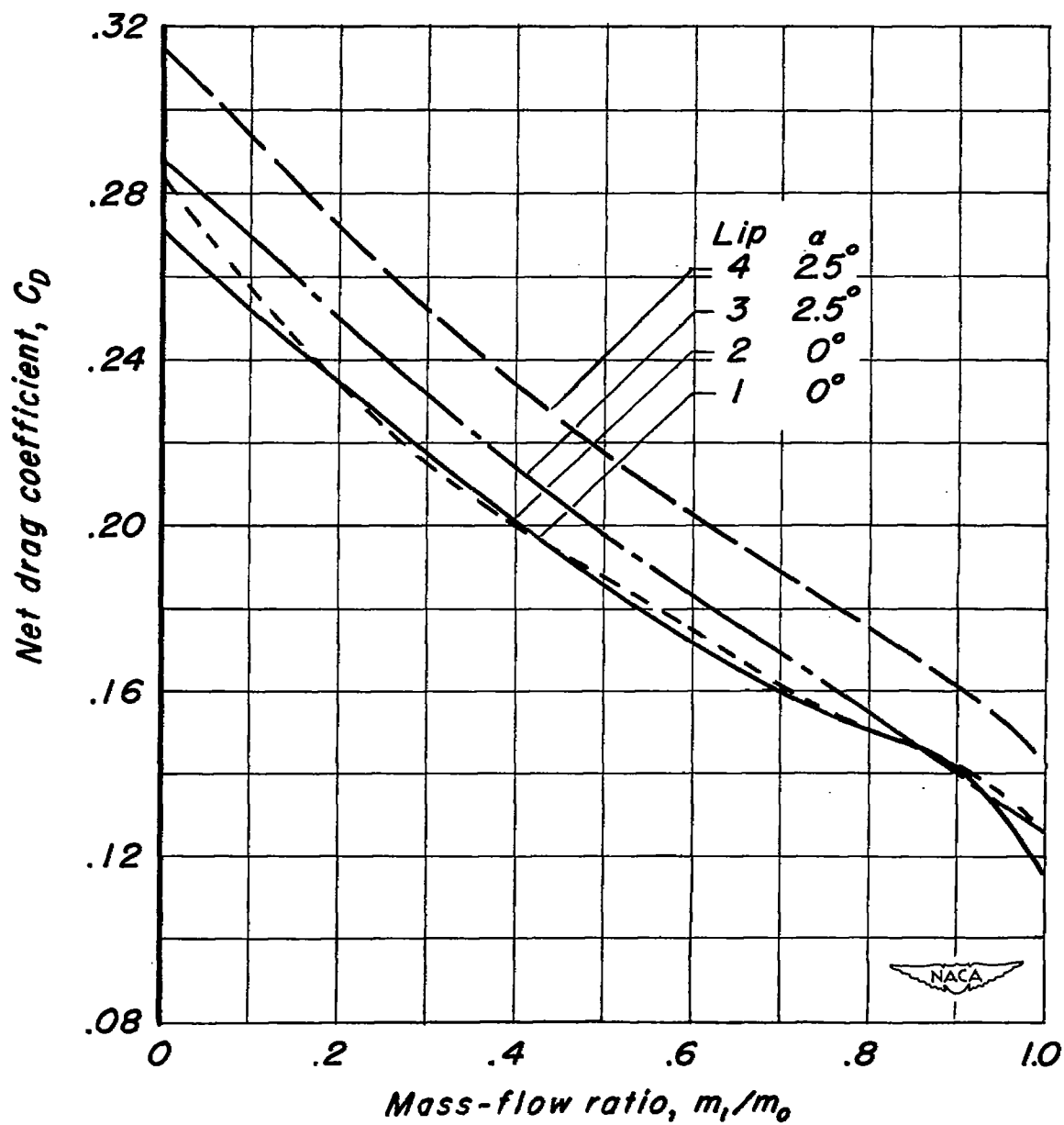
(b)  $M_0 = 1.35$ 

Figure 9.- Continued.

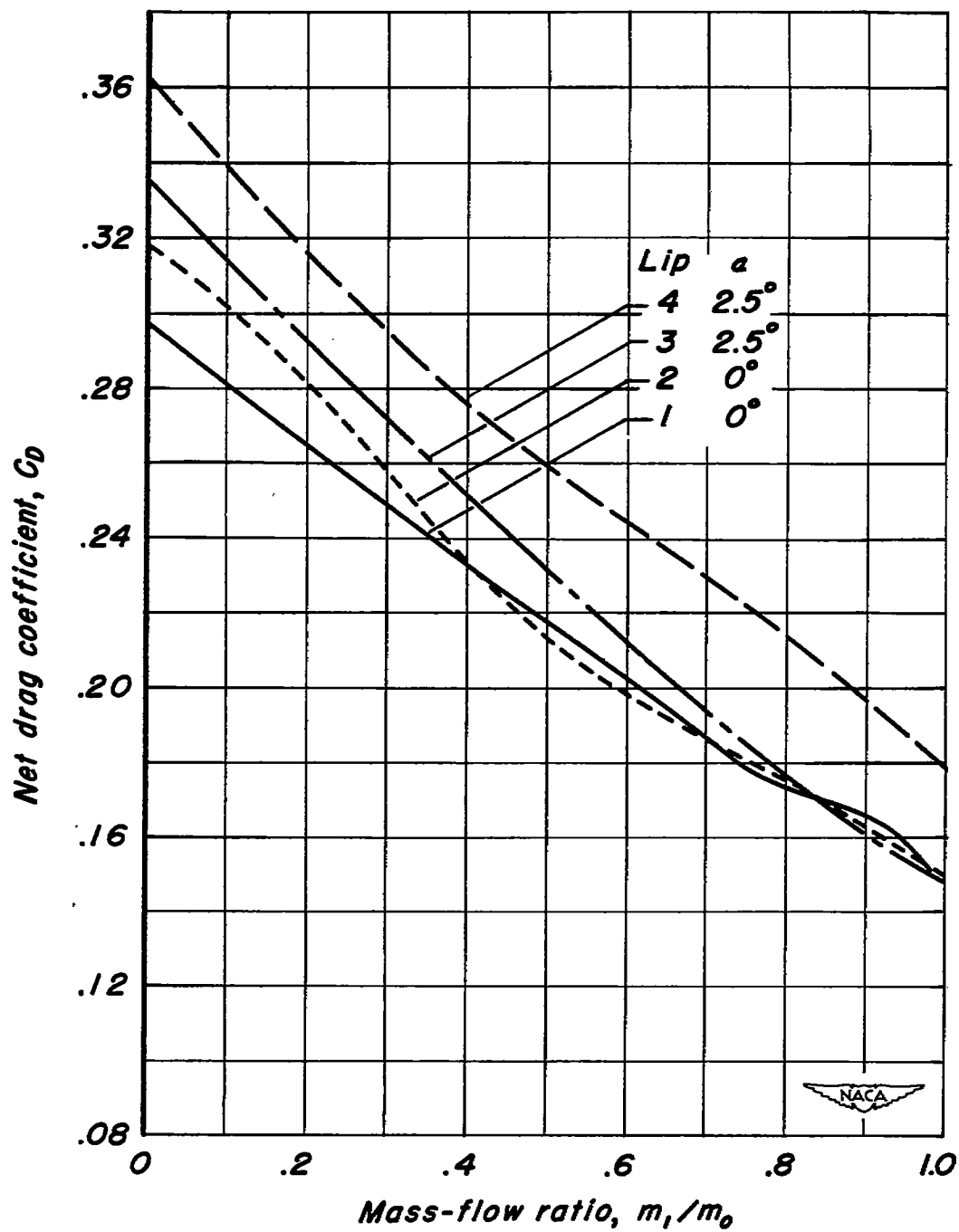
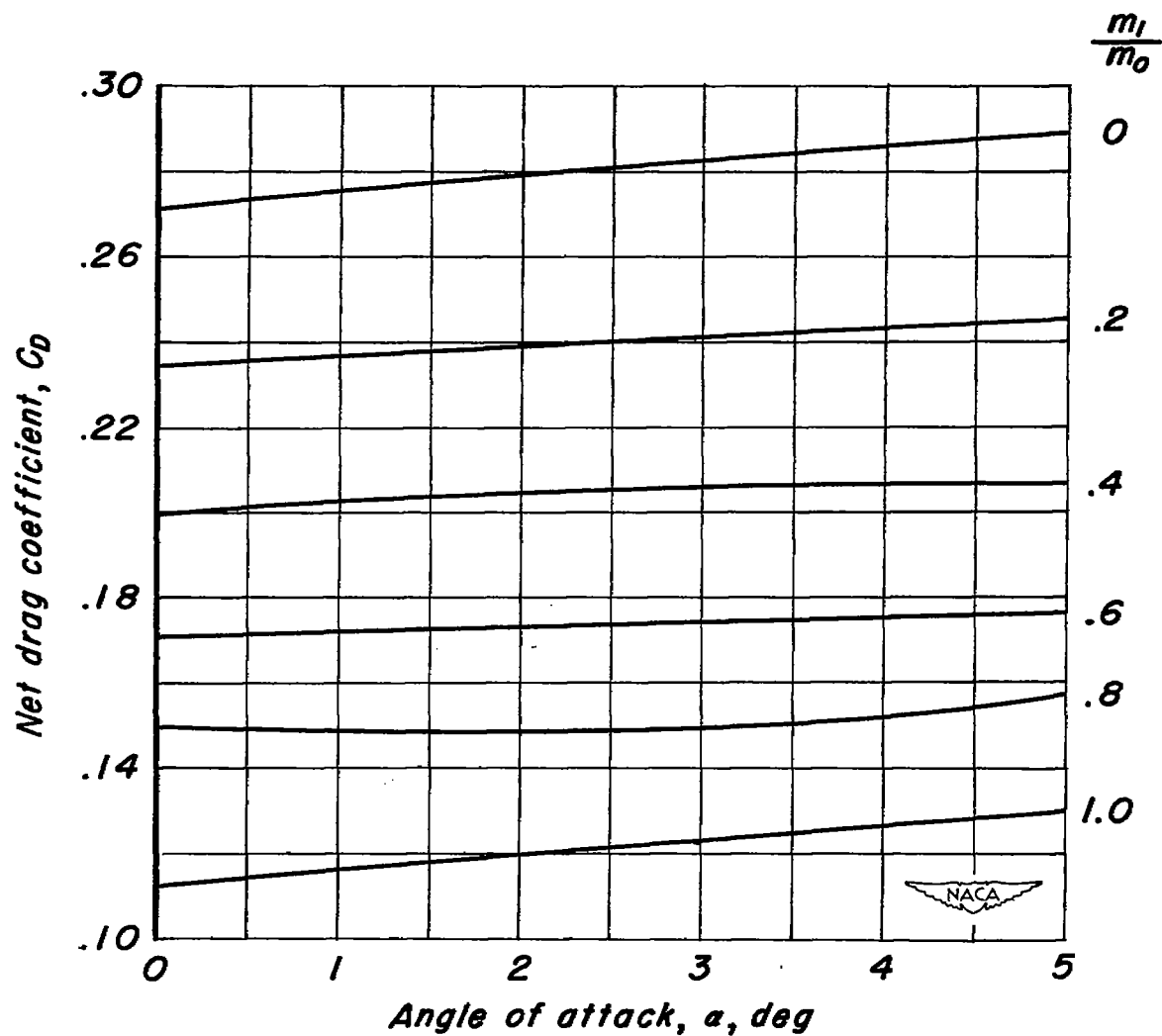
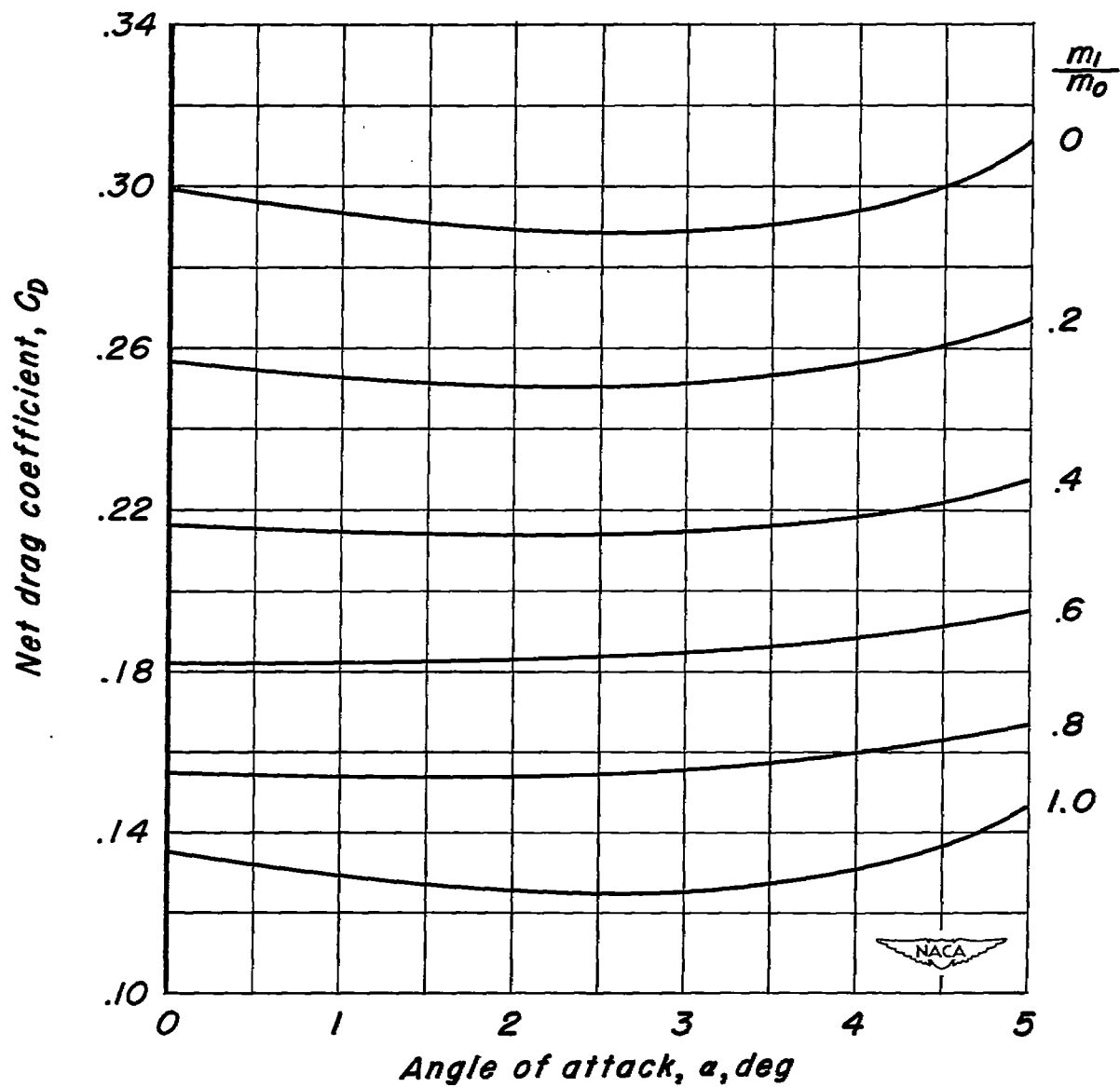
(c)  $M_0 = 1.50$ 

Figure 9.- Concluded.



(a) Lip 2

Figure 10.- The effect of angle of attack on the net drag coefficient for a range of mass-flow ratios;  $M_0 = 1.35$ .



(b) Lip 3

Figure 10.- Concluded.

$$m_1/m_0 = 0.50$$



$$m_1/m_0 = 0.85$$



$$m_1/m_0 = \max$$



A-18848

(a) Lip 2,  $\alpha = 0^\circ$ Figure 11.- Schlieren photographs;  $M_0 = 1.35$ .~~CONFIDENTIAL~~

$$m_1/m_0 = 0.50$$



$$m_1/m_0 = 0.85$$



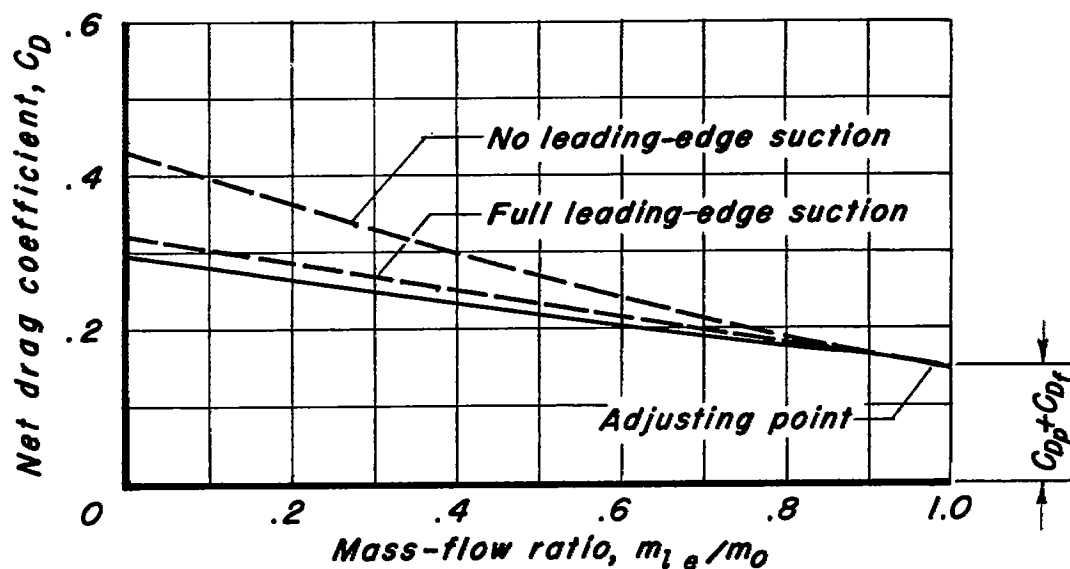
$$m_1/m_0 = \text{max}$$



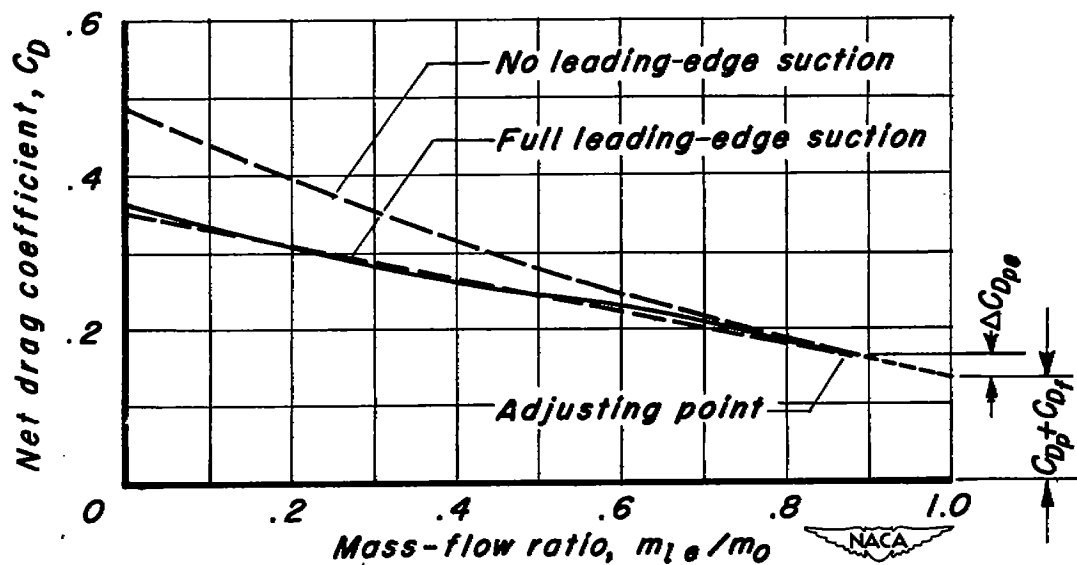
A-18849

(b) Lip 3,  $\alpha = 2.5^\circ$ 

Figure 11.- Concluded.



(a) Lip 1



(b) Lip 4

Figure 12.- A comparison of experimental and estimated net drag coefficient;  $M_0 = 1.5$ .

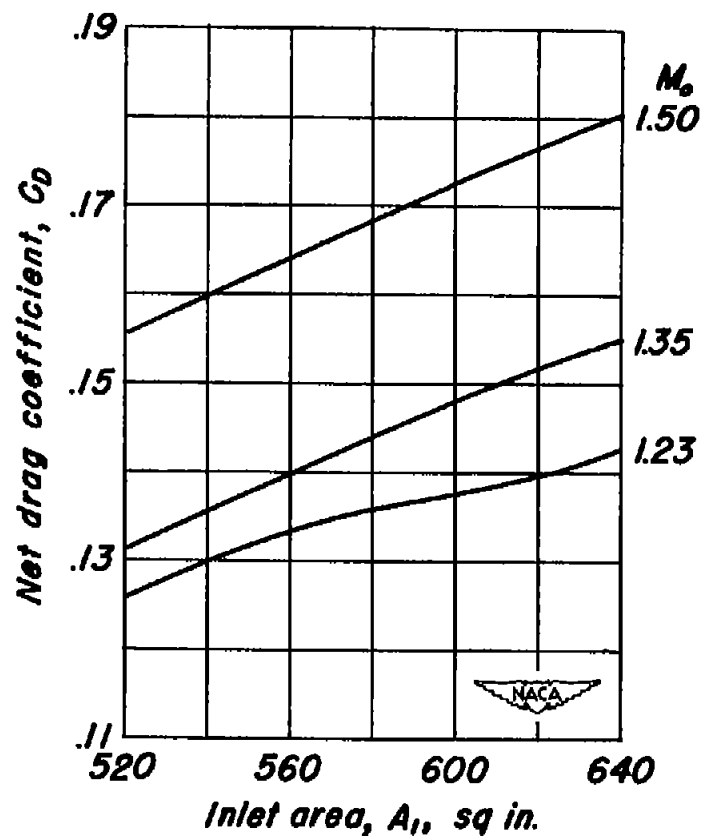
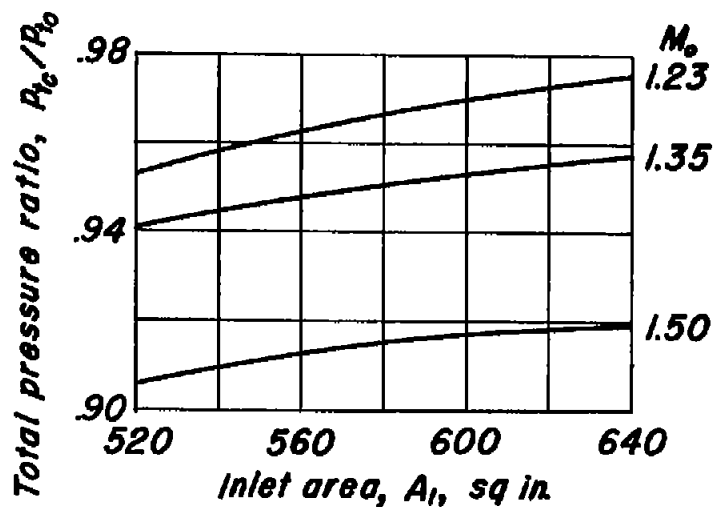
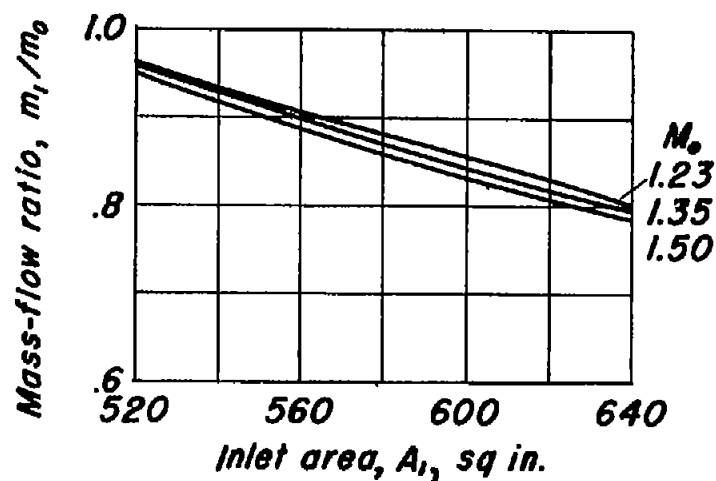


Figure 13.- Pressure recovery, drag, and air-flow characteristics of an inlet-engine combination as a function of inlet area; lip 3,  $\alpha = 2.5^\circ$ , 35,000 feet altitude, military power plus afterburning.

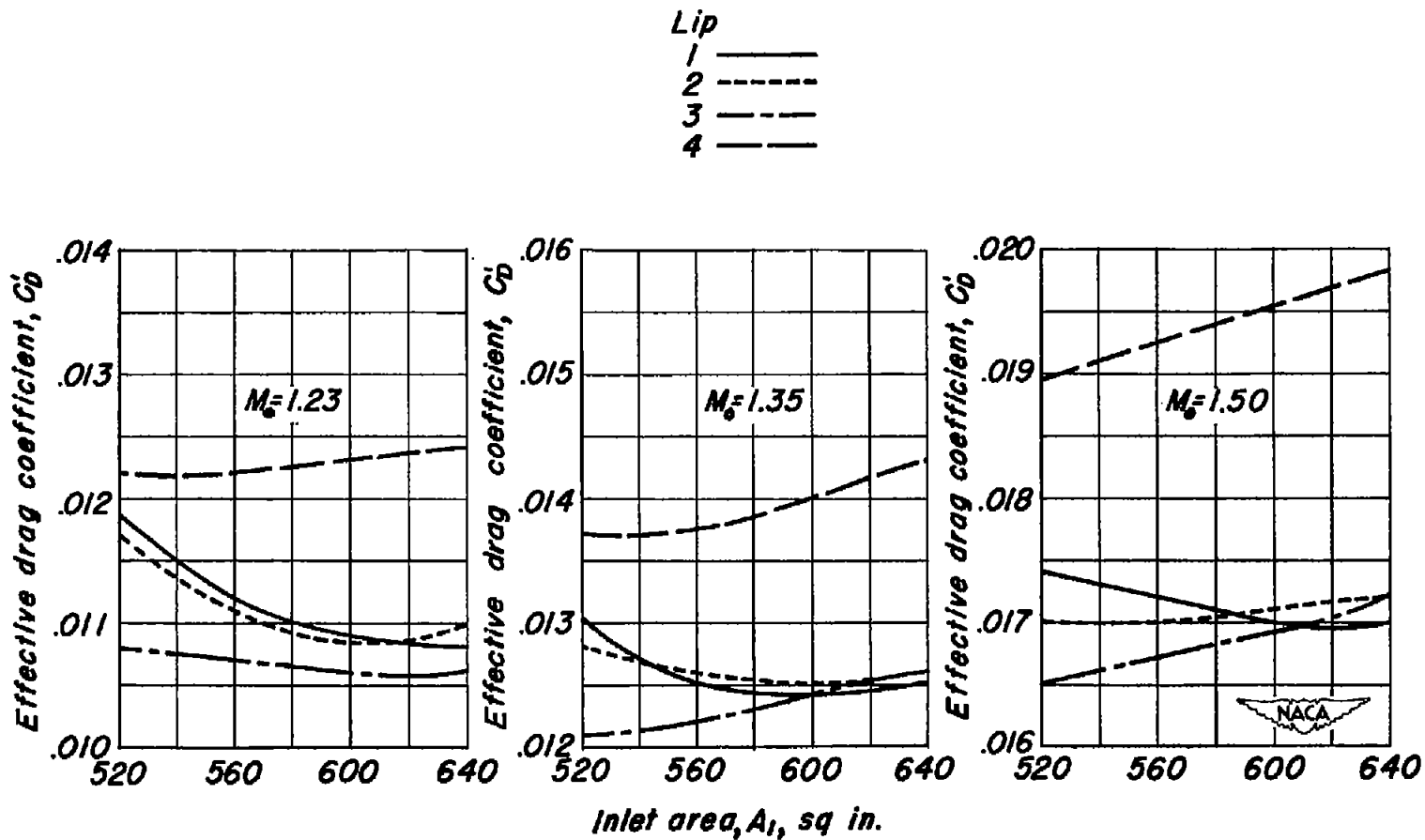


Figure 14.- Effective drag coefficient as a function of inlet area for an inlet-engine combination; altitude = 35,000 feet, military power plus afterburning.

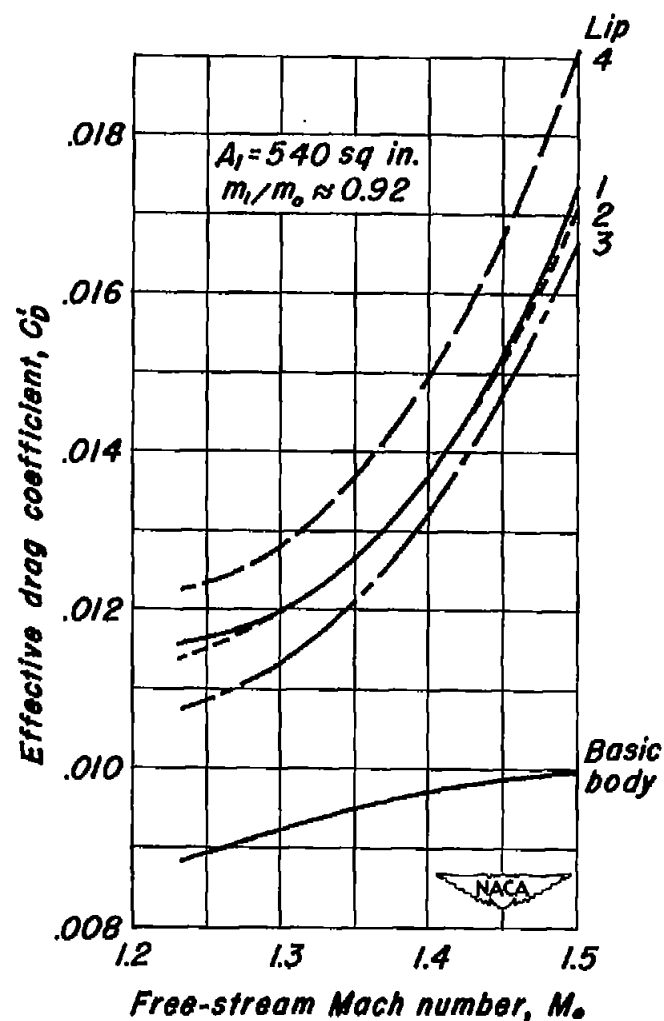
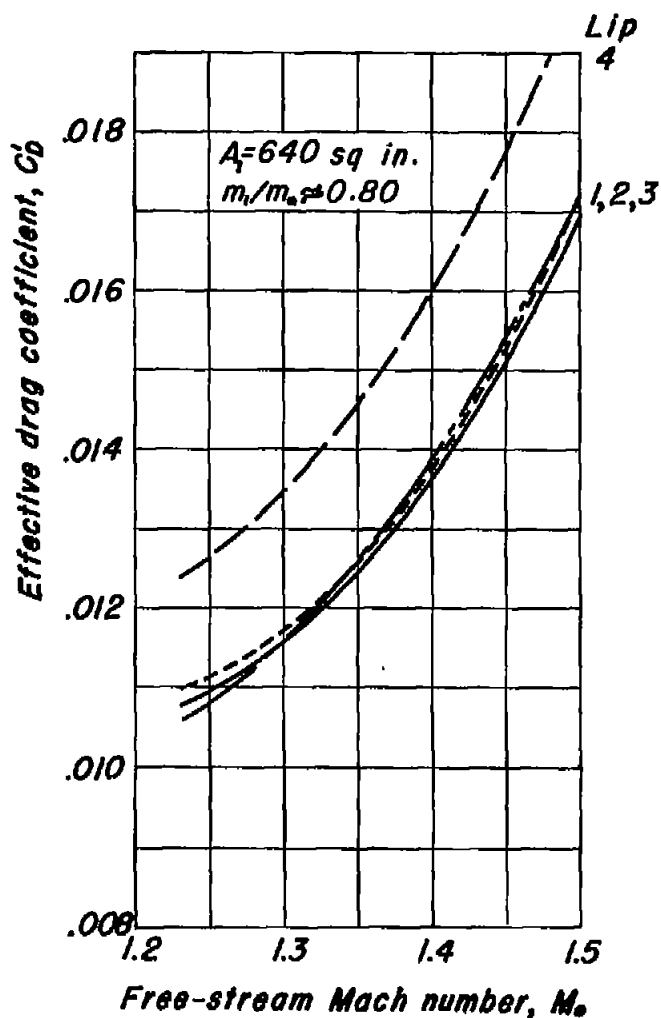
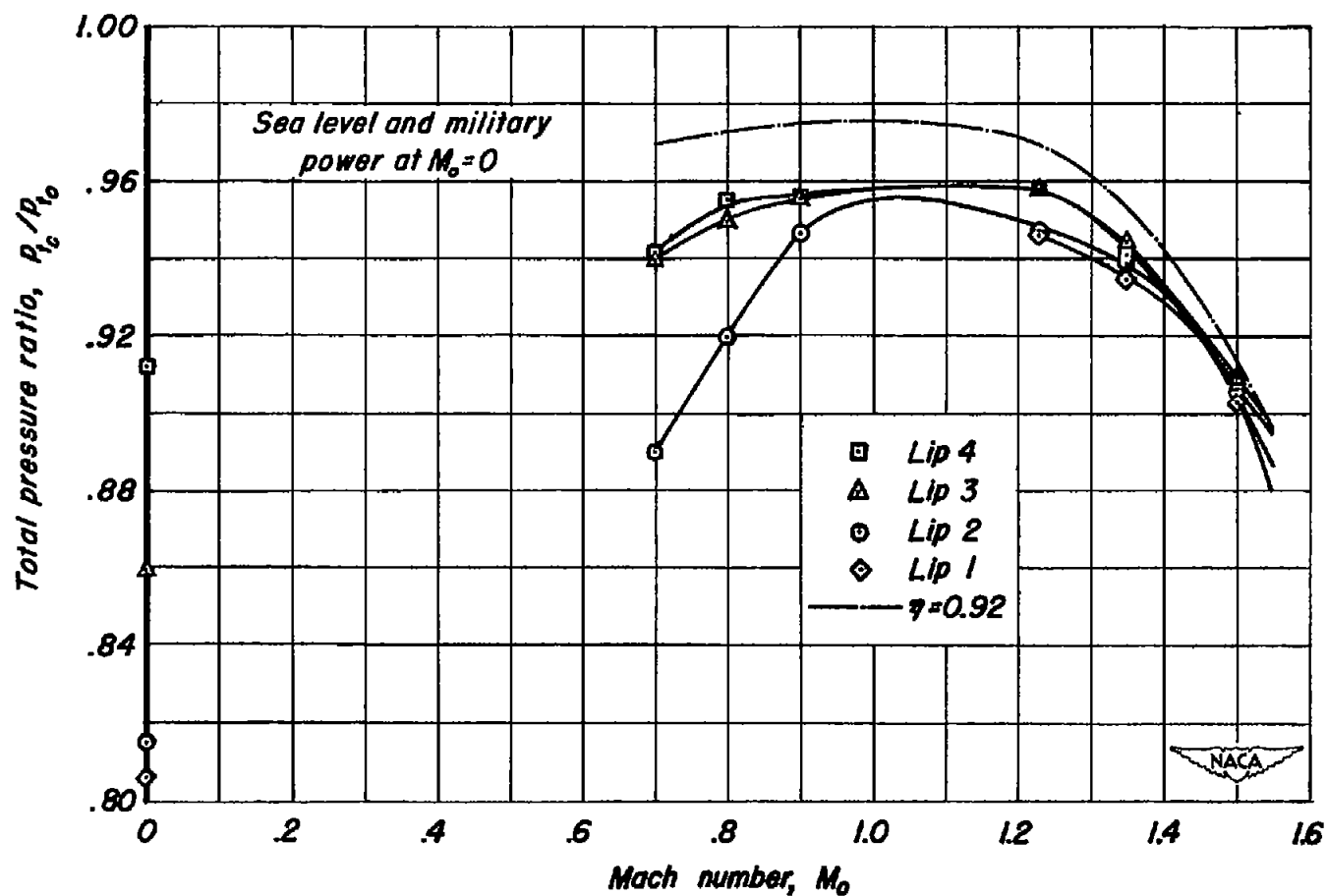
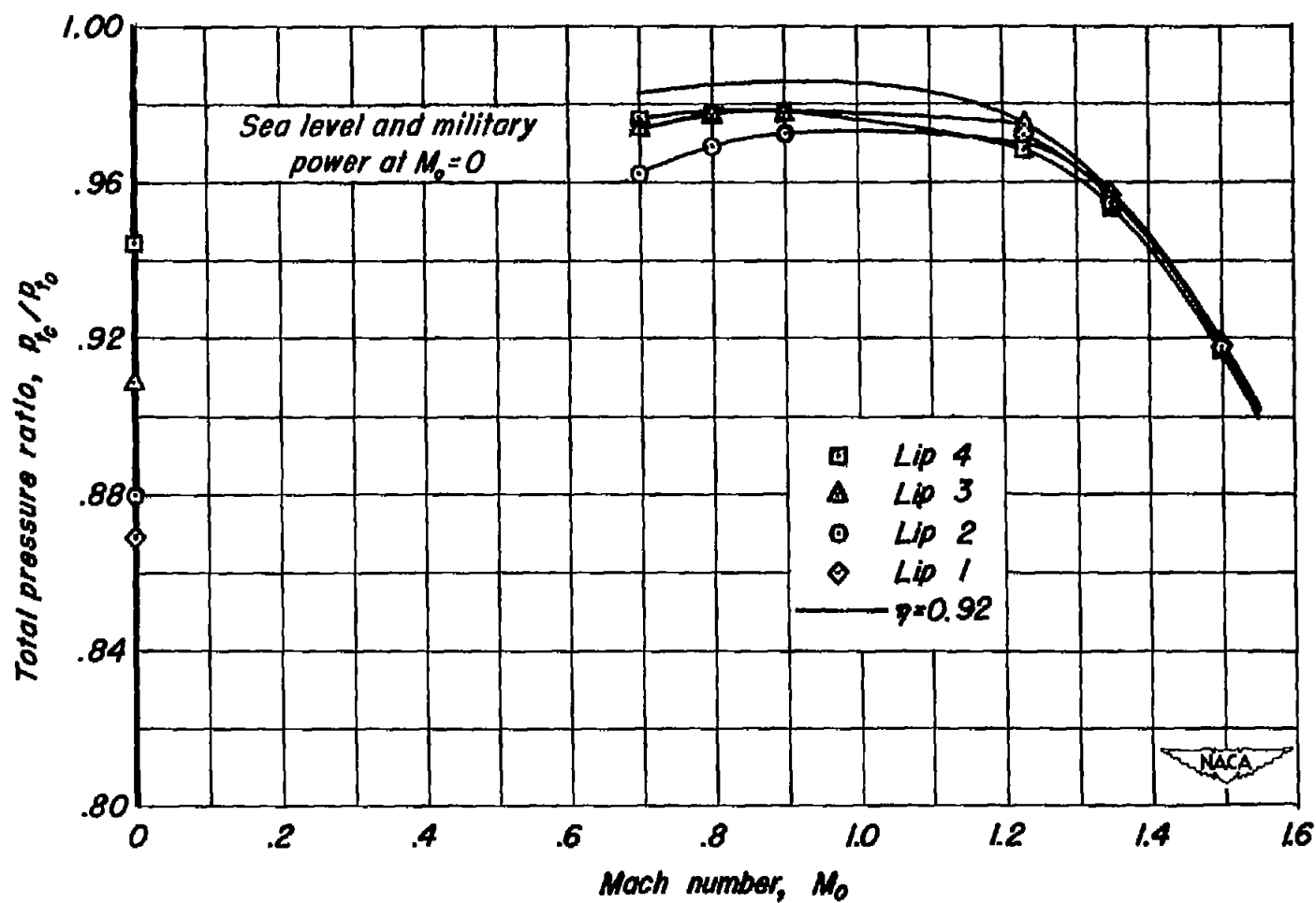


Figure 15.- The effect of Mach number on the effective drag coefficient for two inlet areas; 35,000 feet altitude, military power plus afterburning.



(a)  $A_1 = 540$  sq in.,  $\frac{m_1}{m_0} \approx 0.92$

Figure 16.- The variation of pressure-recovery ratio with Mach number for two design inlet areas; 35,000 feet, military power plus afterburning.



(b)  $A_1 = 640$  sq in.,  $\frac{m_1}{m_0} \approx 0.80$

Figure 16.- Concluded.

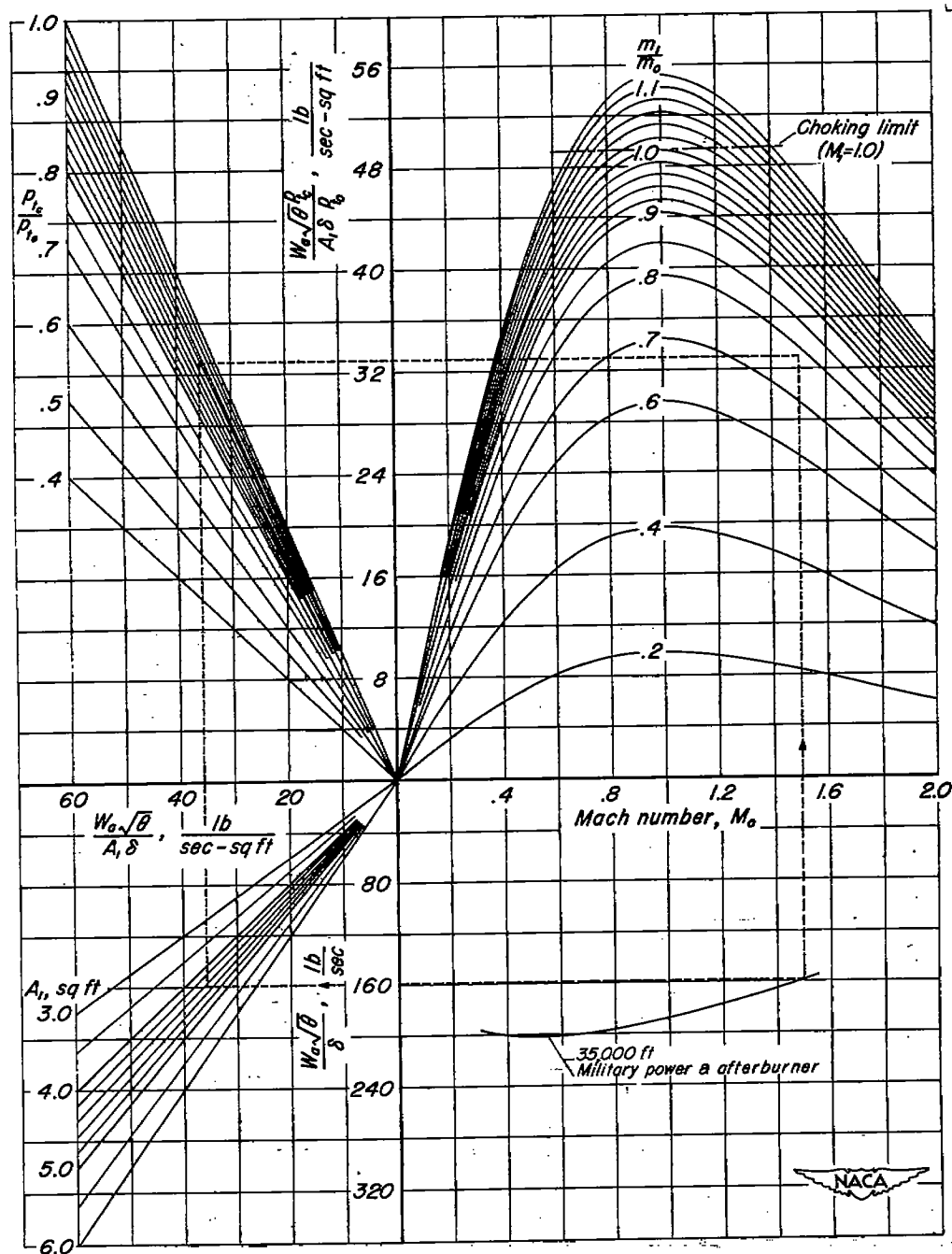


Figure 17.- Nomogram for evaluating the optimum operational characteristics of a combination of an air-induction system and an engine (J-57 jet engine shown as an example).

**CONFIDENTIAL**



**CONFIDENTIAL**